VUV Absorption Spectra of Gas-Phase Quinoline in the 3.5–10.7 eV Photon Energy Range

Sydney Leach, Nykola C. Jones, Søren V. Hoffmann, Sun Un

VUV Absorption Spectra of Gas-Phase Quinoline in the 3.5−10.7 eV Photon Energy Range

Published as part of The Journal of Physical Chemistry virtual special issue "William M. Jackson Festschrift".

Sydney Leach,*[,†] Nykola C. Jones,[‡] Søren V. Hoffmann,[‡] and Sun Un[§]

[†]LERMA, Observatoire de Paris, PSL Research University, CNRS, Sorbonne Universités, UPMC Univ. Paris 06, 92195 Meudon Cedex, France

[‡]ISA, Department of Physics and Astronomy, Aarhus University, 8000 Aarhus C, Denmark

[§]Institute for Integrative Biology of the Cell, Department of Biochemistry, Biophysics and Structural Biology, Université Paris-Saclay, CEA, CNRS UMR 9188, Gif-sur-Yvette 91198, France

ABSTRACT: The absorption spectrum of quinoline was measured in the gas phase between 3.5 and 10.7 eV using a synchrotron photon source. A large number of sharp and broad spectral features were observed, some of which have plasmon-type collective π-electron modes contributing to their intensities. Eight valence electronic transitions were assigned, considerably extending the number of $\pi-\pi^*$ transitions previously observed mainly in solution. The principal factor in solution red-shifts is found to be the Lorentz−Lorenz polarizability parameter. Rydberg bands, observed for the first time, are analyzed into eight different series, converging to the D_0 ground and two excited electronic states, namely, D_3 and D_4, of the quinoline cation. The R1 series limit is 8.628 eV for the first ionization energy of quinoline, a value more precise than previously published. This value, combined with cation electronic transition data, provides precise energies, respectively, 10.623 and 11.355 eV, for the D_3 and D_4 states. The valence transition assignments are based on density functional theory (DFT) calculations as well as on earlier Pariser−Parr−Pople (P−P−P) self-consistent field linear combination of atomic orbitals molecular orbital results. The relative quality of the P−P−P and DFT data is discussed. Both are far from spectroscopic accuracy concerning electronic excited states but were nevertheless useful for our assignments. Our time-dependent DFT calculations of quinoline are excellent for its ground-state properties such as geometry, rotational constants, dipole moment, and vibrational frequencies, which agree well with experimental observations. Vibrational components of the valence and Rydberg transitions mainly involve C−H bend and C═C and C═N stretch modes. Astrophysical applications of the vacuum UV absorption of quinoline are briefly discussed.

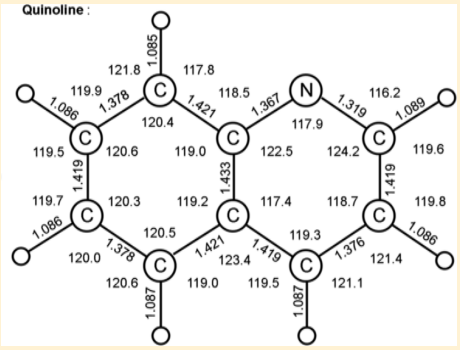

I. INTRODUCTION

The aza-arene quinoline contains a benzene ring fused to a pyridine molecule. It is analogous to naphthalene and is indeed one of the smallest examples of polycyclic aromatic nitrogen heterocycles (PANHs), the nitrogen analogues of the polycyclic aromatic hydrocarbons habitually denoted as PAHs. PANHs have been observed or suspected to exist in planetary atmospheres,[1] the interstellar medium,[2−4] and other astrophysical sites.[4−6] The spectroscopic properties of quinoline, in particular in the gas phase, is thus of potential interest in astrophysical studies and observations, as well as for cosmochemical theoretical simulations.

Quinolines have also quite extensive chemical, biological, and practical uses,[7] as catalysts and corrosion inhibitors in metallurgical processes, in the manufacture of dyes, and as a solvent for resins and terpenes, although their main use is as a feedstock in the production of other chemicals.[8] Quinoline is also used as an antimalarial medicine.[9]

Although there have been many studies of absorption spectra of quinoline in the near-UV region, mainly in solution or in matrices, there have been few studies of its gas-phase absorption spectra. Extensive work has been done on its fluorescence and phosphorescence spectra.[10] Measurements of the absorption spectra of quinoline in the period of 1922−1943 are cited by Ewing and Steck[11] in their pioneer modern study of the effects of solvent pH on these spectra. The earliest gas-phase absorption spectrum, which dates from 1910,[12] is a photographic plate spectrum of quinoline absorption in which, using a cadmium spark as a quasi-continuum source, a broad band was observed in the near-ultraviolet (band wavelengths not specified). The more recent gas-phase absorption measurements of quinoline[10,13−15] are restricted to the near-UV in the 3.8−4.5 eV region, while solution absorption spectra

of quinoline have an upper photon energy limit of ~5.4 eV.[10,16,17] An absorption spectrum of liquid quinoline up to 10.6 eV has also been measured.[18]

The Aarhus synchrotron radiation source enabled us to extend absorption spectral measurements of *gas-phase* quinoline up to 10.7 eV, to identify eight valence transitions, to discover eight previously unknown Rydberg series of bands converging to ground and excited electronic states of the ion, and to measure the absorption cross sections over the 3.6–10.7 eV region, of crucial importance in cosmochemical process modeling.

II. EXPERIMENTAL SECTION

II.1. Absorption Measurements. The absorption measurements were performed on the AU-UV beamline at the ASTRID2 synchrotron facility in Aarhus, Denmark. A detailed description of the AU-UV beamline, its resolution possibilities, and procedure for determining absorption cross sections is given by Palmer et al.[19] The quinoline samples were introduced at room temperature into a gas cell with a path length (l) of 15.5 cm, whose entrance and exit MgF_2 windows are effectively transparent in the vacuum ultraviolet (VUV) down to ~10.8 eV (115 nm). A toroidal dispersion grating provided VUV radiation at selective energies; wavelength scans were performed with step sizes ranging from 0.05 to 0.2 nm, chosen according to the level of structure in different regions of the spectrum. The intensity of the light transmitted through the gas (I_t) is measured by a UV–VUV sensitive photomultiplier (ET Enterprises 9406B). There is a small gap between the exit window of the gas cell and the recording photomultiplier. This gap is evacuated, thus preventing air contamination, to maintain transparency at photon energies above 5.5 eV. At lower energies, air is allowed into this gap to remove higher-order radiation, while the MgF_2 entrance window of the cell prevents higher-order radiation above 11 eV. Gas pressure is measured by a heated baratron capacitance manometer (Inficon CDG100D). The synchrotron beam current is measured during each wavelength scan, and the measured intensity is normalized to this current. A background scan is recorded with the cell evacuated (I_o).

Absorption cross sections were determined, with a general accuracy of ±5%, using the Beer–Lambert law: $I_t = I_0 \exp(n\sigma l)$. The quinoline sample, of highest purity commercially available (Sigma-Aldrich), was prepared for use with four freeze–pump–thaw cycles and used without further treatment.

II.2. Computational Methods and Results. Quinoline is a heterocyclic planar molecule belonging to the C_s symmetry group. We are interested in calculations of the valence transitions of quinoline to aid in spectral transition assignments, the π–π^* transitions, in particular. There are many reported quantum mechanical computations of these quantities, mainly by Pariser–Parr–Pople (P–P–P) methods as discussed in Section III.1. We found these useful for spectral assignments but thought it worthwhile to perform time-dependent density functional theory (TD-DFT) calculations for comparison. We note that the TD-DFT formalism derived from Kohn–Sham theory can also be considered as an empirically corrected variant of the random-phase approximation (RPA) in Hartree–Fock theory.[20,21]

Our quantum chemical calculations were performed using the Gaussian 09 program, revision C.01.[22] Initial geometry optimization of quinoline was performed using the hybrid density functional B3LYP and 6-31+G(d,p) basis set. Normal mode analysis confirmed that the final optimized geometry was a true potential energy minimum. This structure was used to perform TD-DFT using the CMB3LYP hybrid density-functional[23] and the 6-31+G(d,p) basis-set.

II.2.1. Structural Properties. There are no reported direct measurements of the geometry of quinoline, but our calculated structural parameters (Figure 1) are in satisfactory agreement

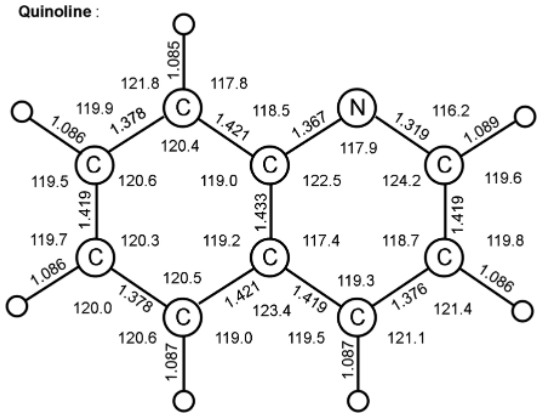

Figure 1. Calculated geometry of quinoline. Bond distances (Å) and angles (deg) calculated by a TD-DFT method.

with other calculated values.[24–27] Experimental values of gas-phase ground-state rotational constants are known from high-resolution microwave and/or optical spectroscopy measurements.[26–29] Our calculated rotational constants are in quite good agreement with the experimental values for quinoline (Table 1). Another criterion of quality for the ground electronic state is the dipole moment. Our calculated values of the dipole moment are in very good agreement with quinoline values obtained from gas-phase polarization measurements,[30] but are ~12% larger than the Stark effect values (Table 1). Determining the dipole moment from polarization measurements in the gas phase requires measurements that extend over a temperature range of at least 100 K. This condition was fulfilled in the measurements of Buckingham et al.[30] Uncertainties in Stark effect measurements of gas-phase dipole moments are discussed by Kisiel et al.[26] A wide range of calculated values of the dipole moment of quinoline given by a varied set of quantum mechanical

Table 1. Calculated and Experimental Physical Properties of Quinoline

I. Quinoline Rotational Constants:

(a) DFT-calculated rotational constants (present study):

A = 3.140 8386 GHz, B = 1.265 7855 GHz, C = 0.902 1936 GHz

(b) microwave spectroscopy (Kisiel et al.[26]):

A = 3.145 533 013 GHz, B = 1.271 577 972 GHz, C = 0.905 739 406 GHz

(c) microwave and FIR spectroscopy (Pirali et al.[28]):

A = 3.145 533 064 GHz, B = 1.271 578 102 GHz, C = 0.905 739 476 GHz

II. Quinoline Dipole Moment:

(a) DFT-calculated dipole moment: 2.2254 D (present study)

(b) gas-phase dipole moment from polarization measurement (Buckingham et al.[30]): 2.27 ± 0.05 D

(c) gas-phase dipole moment from Stark effect measurement (Kisiel et al.[26]): 2.0197 D

Table 2. Quinoline Vibrational Frequencies (cm^{-1}): Harmonic Frequency Calculations cf. Observed Values

vibrational mode[32]	observed[32]	DFT harmonic present study	DFT harmonic[29]	Hartree−Fock[24]	force field refinement[25]
1 a′	3085	3214	3196	3383	3155
2 a′	3056	3207	3188	3377	3068
3 a′	3056	3202	3183	3368	3068
4 a′	3036	3188	3167	3352	3061
5 a′	3015	3179	3160	3347	3059
6 a′	3005	3175	3157	3339	3058
7 a′	2982	3158	3133	3329	3056
8 a′	1619	1667	1656	1837	1625
9 a′	1597	1644	1634	1812	1592
10 a′	1571	1610	1601	1784	1564
11 a′	1500	1544	1532	1674	1531
12 a′	1471	1501	1492	1632	1461
13 a′	1431	1471	1459	1594	1405
14 a′	1392	1424	1414	1537	1382
15 a′	1371	1399	1387	1487	1358
16 a′	1316	1369	1355	1455	1328
17 a′	1257	1284	1276	1387	1251
18 a′	1217	1263	1257	1365	1219
19 a′	1192	1241	1232	1304	1188
20 a′	1143	1174	1166	1262	1141
21 a′	1119	1166	1158	1246	1112
22 a′	1095	1144	1136	1197	1094
23 a′	1034	1055	1046	1116	1059
24 a′	1013	1037	1031	1073	1030
25 a′	956	950	947	1028	999
26 a′	785	796	825	884	985
27 a′	760	771	767	832	948
28 a′	612; 611[29]	640	621	664	639
29 a′	522	530	527	571	517
30 a′	(505)	527	525		480
31 a′	380; 375[29]	381	379	407	379
32 a″	986	1003	1001	1126	999
33 a″	971	999	994	1121	985
34 a″	940	973	970	1094	942
35 a″	868	968	964	1090	865
36 a″	850	882	886	979	823
37 a″	806	821	820	908	766
38 a″	786	796	804	879	743
39 a″	741	748	748	830	675
40 a″	629; 628[29]	640	643	696	619
41 a″	479; 476[29]	493	489	540	481
42 a″	472	479	478	523	420
43 a″	393; 389[29]	403	400	441	339
44 a″	192; 178[28]	184	183	206	195
45 a″	178; 168[28]	175	173	192	118

methods has recently been listed and discussed by Ebenso et al.[31]

II.2.2. Ground-State Vibrational Frequencies. Our DFT study included calculations of the ground-state harmonic and anharmonic vibrational frequencies of quinoline. The results on the 31 a′ symmetry and 14 a″ vibrational modes, compared with the experimental values of Wait and McNerney[32] and with other calculations of quinoline vibrational frequencies, are presented in Tables 2 and 3, used for general interest as comparative tests for various calculation methods of vibrational frequencies. The experimental frequencies reported by Wait and McNerney are from their infrared and Raman study in liquid- and/or in gas-phase quinoline. Mode assignments were made on the basis of normal coordinate analysis using the Urey−Bradley force field including Kekulé modification with force constants transferred from naphthalene and *s*-triazine. High-resolution gas-phase far-infrared spectroscopy, performed by Martin-Drumel et al.[29] with a Fourier transform instrument also provided frequencies for modes 28, 31, 40, 41, 43, and 45. Millimeter-wave spectroscopy was used by Pirali et al.[28] to obtain high-resolution gas-phase values for the frequencies of modes 44 and 45.

Table 2 also includes the results of a force-field and vibrational spectral study of quinoline whose geometry was optimized at the Hartree−Fock level of theory using a 6-31G** basis set, performed by Bandyopadhyay and Manogaran.[24] The ab initio values of the vibrational frequencies, given in the table, require severe scaling (0.7−1.0 for a′ modes and

Table 3. Quinoline Vibrational Frequencies (cm^{-1}): Anharmonic Frequency DFT Calculations cf. Observed Values

vibrational mode[32]	observed[32]	B97−1 6-311+G(d,p)	B97−1 6-311G(d,p)	B97−1 6-311G(d,p)[29]	B3LYP 6-311+G(d,p)	B3LYP 6-31+G(d,p)
1 a′	3085	3077	3080	3064	3076	3067
2 a′	3056	3057	3058	3055	3059	3075
3 a′	3056	3067	3052	3060	3049	3095
4 a′	3036	3038	3040	3044	3037	3052
5 a′	3015	3033	3039	3041	3039	3055
6 a′	3005	3000	3010	3007	3010	3021
7 a′	2982	3012	3000	3011	3015	3031
8 a′	1619	1613	1616	1615	1616	1626
9 a′	1597	1594	1596	1597	1599	1608
10 a′	1571	1561	1562	1563	1565	1572
11 a′	1500	1493	1495	1496	1500	1508
12 a′	1471	1464	1466	1466	1473	1475
13 a′	1431	1427	1428	1428	1434	1438
14 a′	1392	1386	1386	1387	1392	1397
15 a′	1371	1354	1352	1364	1355	1367
16 a′	1316	1321	1322	1322	1324	1335
17 a′	1257	1249	1249	1250	1257	1260
18 a′	1217	1230	1232	1232	1236	1238
19 a′	1192	1216	1218	1213	1221	1226
20 a′	1143	1149	1150	1149	1156	1160
21 a′	1119	1141	1142	1143	1148	1151
22 a′	1095	1119	1119	1119	1125	1127
23 a′	1034	1027	1028	1028	1034	1037
24 a′	1013	1012	1013	1013	1017	1020
25 a′	956	933	934	934	940	937
26 a′	785	814	814	814	819	818
27 a′	760	754	755	755	759	760
28 a′	612; 611[29]	614	614	614	620	618
29 a′	522	521	521	521	524	524
30 a′	(505)	519	520	520	522	522
31 a′	380; 375[29]	375	375	375	380	379
32 a″	986	978	977	977	985	981
33 a″	971	981	978	978	985	980
34 a″	940	953	952	951	958	954
35 a″	868	950	948	949	951	953
36 a″	850	872	868	866	875	898
37 a″	806	807	807	808	807	814
38 a″	786	783	788	787	785	797
39 a″	741	733	734	735	734	733
40 a″	629; 628[29]	628	633	631	632	643
41 a″	479; 476[29]	480	481	480	484	485
42 a″	472	468	469	467	472	482
43 a″	393; 389[29]	391	493	392	394	395
44 a″	192; 178[28]	176	179	178	178	180
45 a″	178; 168[28]	170	172	170	171	173

0.5−1.0 for a″ modes) to bring them in line with observed values. An evaluation of various ab initio, semiempirical, and DFT methods of calculation of molecular harmonic vibrational frequencies has been made to determine optimal frequency scaling factors.[33,34] The final right-hand column in Table 2 gives the results of a theoretical study by Özel et al.[25] using a force-field refinement method in which the force-field parameters of quinoline were determined by refinement of the corresponding parameters of benzene and pyrimidine molecules, taking into account the results of semiempirical and ab initio calculations. This gave frequency values in very reasonable agreement with observed values for many, but not all, vibrational modes. A comparison of the calculated frequencies in the various studies represented in Table 2 shows that the DFT harmonic calculations provide reasonable values that require far less scaling or refinement techniques to simulate observed values, consistent with the conclusions of the study of Scott and Radom.[34]

It is well-known that harmonic vibrational frequencies derived from DFT calculations require scaling. The B3LYP/6-31+G(d,p) anharmonic frequencies calculated using the second-order vibrational perturbation theory implemented by Barone[35] in Gaussian 09 required essentially no scaling (Table 3). The root-mean-squared deviation of these anharmonic values from the observed was 23 cm^{-1} with a maximum absolute deviation of 85 cm^{-1}. They were in general closer in value than those obtained by Martin-Drumel et al.[29] with the hybrid B97-1 functional and the 6-311G(d,p) basis set. This

appeared to be largely due to the different implementations of the second-order vibrational perturbation theory in the two different versions of Gaussian used. When the B97-1/6-311G(d,p) anharmonic frequencies were recalculated using the method of Barone,[35] their correlation to the observed values was markedly improved and was only statistically slightly worse than those using B3LYP/6-31+G(d,p). Better results were obtained using B97-1/6-311+G(d,p) with a root-mean-squared deviation of 17 cm^{-1} and a maximum deviation of 82 cm^{-1}. Thus, as expected, the results of DFT anharmonic calculations come closer to experimental values and can generally be more useful in vibrational mode assignments.

II.2.3. Electronic State Energies and Transition Oscillator Strengths. The energies and oscillator strengths of transitions to the first 33 singlet electronic excited states of quinoline up to 8.214 eV (13 A′ states, 19 A″ states) were calculated using the TD-DFT method[20] with the same hybrid density function and basis set. The eigenvalues are critically dependent on molecular orbital (MO) energy differences in TD-DFT calculations, so that the calculations may not provide reliable values for transition energies. This has proved to be the case as discussed later in the valence transition assignments of the absorption spectra of quinoline. However, these calculations enable us to differentiate between strong and weak electronic transitions, since DFT-calculated oscillator strengths are not very sensitive to the exactness of calculated transition energies,[36,37] thus facilitating certain aspects of the valence transition assignments. However, particular transition oscillator strengths can be distorted if there is interaction with plasmon-type effects (see later). The calculated transition energies and oscillator strengths are listed in Table 4.

III. RESULTS AND DISCUSSION

III.1. Quinoline VUV Absorption Spectrum. The complete absorption spectrum of gas-phase quinoline between 3.6 and 10.7 eV is given in Figure 2. It includes a 10× intensity magnification insert between 3.8 and 5.6 eV. The spectrum is very rich in features, many of which are small peaks lying on diffuse continua, and some are present as shoulders in the absorption signal. The 137 measured features can be seen in more detail in intensity zooms of various sections of the absorption spectrum. Typical examples are given in Figures 3–8 for the spectral regions of 3.5–5.0, 4.5–5.8, 5.5–6.2, 6.5–7.8, 7.5–8.7, and 8.5–10.7 eV, respectively. Measurement of band energies was based on clear peaks evidenced as maxima in the recorded absorption cross sections as well as gradients in the cross sections in cases of less well-resolved features. The precision of peak energy pointing was between ±0.0006 and ±0.004 eV, depending on the spectral range and the step size in the wavelength scan. The measured features are listed as band numbers, energies, and band assignments in Table 5. These assignments are based, in part, on the results of electronic energy and transition-strength calculations by various quantum-mechanical methods discussed below.

Innes et al.[10] have listed the triplet and singlet energy level energies and strengths of n–π^* and π–π^* transitions of quinoline as evaluated in 1988. Similar data, limited to π–π^* transitions, were published earlier by Baba and Yamzaki[38] in connection with their molecular orbital calculation study of quinoline absorption spectra, using the Pariser–Parr–Pople self-consistent field (SCF) linear combination of atomic orbitals (LCAO) molecular orbital (MO) method. They calculated nine π–π^* transitions up to 7.11 eV, as did Nishimoto,[39] whose SCF MO calculations used a fixed core approximation, while eight calculated transitions in this energy region are reported by Tinland,[40] using the P–P–P SCF LCAO MO method, and by Ridley and Zerner[41] who used a

Table 4. Quinoline. DFT-Calculated Singlet Transition Energies and Oscillator Strengths

transition	transition energy, eV	oscillator strength, *f*
1A″ ← 1A′	4.6228	0.0023
2A′ ← 1A′	4.6484	0.0274
3A′ ← 1A′	4.7312	0.0622
2A″ ← 1A′	5.6923	0.0000
4A′ ← 1A′	6.0226	0.9655
5A′ ← 1A′	6.2419	0.0489
3A″ ← 1A′	6.3132	0.0000
6A′ ← 1A′	6.4344	0.1934
7A′ ← 1A′	6.5980	0.2540
4A″ ← 1A′	6.6941	0.0024
5A″ ← 1A′	6.8215	0.0278
6A″ ← 1A′	6.8419	0.0076
8A′ ← 1A′	6.8529	0.1008
7A″ ← 1A′	6.9287	0.0002
8A″ ← 1A′	7.2017	0.0002
9A′ ← 1A′	7.2399	0.0378
9A″ ← 1A′	7.2866	0.0004
10A″ ← 1A′	7.3051	0.0011
11A″ ← 1A′	7.4243	0.0072
12A″ ← 1A′	7.4698	0.0056
10A′ ← 1A′	7.5841	0.0006
13A″ ← 1A′	7.5996	0.0048
14A″ ← 1A′	7.6699	0.0008
11A′ ← 1A′	7.7013	0.0035
15A″ ← 1A′	7.7300	0.0020
12A′ ← 1A′	7.8613	0.0464
13A′ ← 1A′	7.9459	0.0085
16A″ ← 1A′	7.9466	0.0003
14A′ ← 1A′	7.9979	0.0016
17A″ ← 1A′	8.1113	0.0012
18A″ ← 1A′	8.1521	0.0068
19A″ ← 1A′	8.1903	0.0002
20A″ ← 1A′	8.2142	0.0001

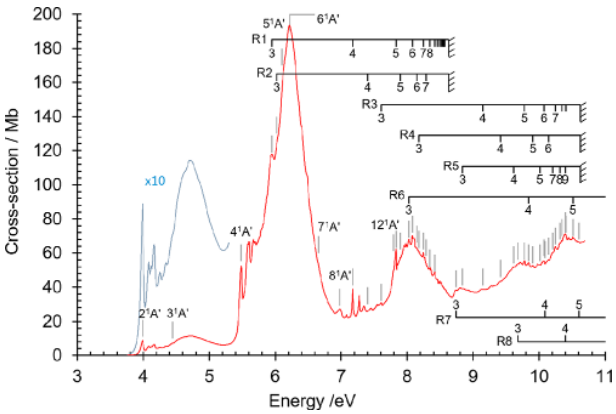

Figure 2. Quinoline absorption spectrum 3.6–10.7 eV. Bands of the Rydberg series R1–R8 are indicated. The O_0^0 origin bands of the successive π–π^* valence transitions $m^1A' \leftarrow 1^1A'$ (Table 5) are indicated as $2^1A' \cdots 12^1A'$. Vibrational components listed in Table 5 are not indicated, for clarity in the figure.

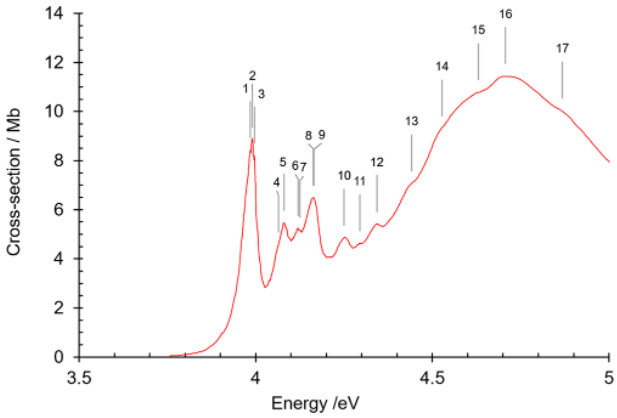

Figure 3. Quinoline absorption spectrum 3.5−5.0 eV. Band numbers are pinpointed.

modified intermediate neglect of differential overlap (INDO) method in their SCF LCAO MO calculations (Table 6). We note that configuration interactions were included in several studies.[38,41,42] More limited $\pi-\pi^*$ transition calculations were performed by Favini et al.[16] and by Mataga[43] to interpret solution spectra, as well as by Wagner et al.[42] who reported three $\pi-\pi^*$ transitions up to 5.78 eV (Table 6), while Goodman and Harrell[44] made analogous calculations on n$-\pi^*$ transitions. The results of these works, and of our own DFT calculations (Table 6), have helped in assigning the various sharp and broad features of quinoline valence transitions in our gas-phase absorption spectrum, which is described below, divided into a number of energy sectors. We also observed Rydberg transition bands for the first time. There are no reported calculations of quinoline Rydberg states.

We base our $\pi-\pi^*$ transition analysis and discussion mainly on the calculations of Baba and Yamakazi,[38] whose transition energies and oscillator strengths are in excellent agreement with those of Nishimoto[39] and in satisfactory agreement with those of Tinland[40] and of Ridley and Zerner.[41] Our DFT-calculated transition energies are consistently greater than those of the older, mainly P−P−P, calculations and were generally found to be less useful for spectral assignment. We note, however, that our DFT calculations indicate that, for quinoline, of the 20 n$-\pi^*$ transitions (Table 4), only one, 5A″−1A′ calculated energy 6.822 eV, f = 0.0278, would have an oscillator strength of sufficient value to be observable in our spectra. These energies correspond to regions of overlying well-assigned Rydberg and valence bands.

III.1.1. Valence Transitions: 3.6−5.4 eV. Transitions to the $2^1A'$ and $3^1A'$ Electronic States. This part of the spectrum has previously been studied in solution and in the vapor phase.

There are structured features in the 3.8−4.6 eV region (Figures 2 and 3). The energy of the initial principal peak, measured at 3.991 eV (32 190 cm^{-1}), is assigned to the $2^1A' \leftarrow 1^1A$ O^0_0 origin (see below). It agrees well with the values of other vapor-phase studies: 32 196 cm^{-1} that we determined from Figure 6 of a published vapor-phase absorption spectrum of quinoline by Okajima and Lim[14] and 32 192 cm^{-1} from a resonance-enhanced two-photon ionization spectrum.[15]

In condensed phases the first peak is shifted to lower energies by amounts, generally less than ∼350 cm^{-1}, dependent on the solvent. These redshifts for quinoline arise, in part, because of possibilities of forming hydrogen bonds with solvents containing −OH groups. Another factor in determining the position of the $2^1A' \leftarrow 1^1A$ origin band concerns displacements due to interaction between the lowest excited n$-\pi^*$ and $\pi-\pi^*$ levels (see below) that will be affected differently in polar and nonpolar solvents. This is linked to the major factor in solvent shifts that is due to the electrostatic work required to produce the solute transition dipole, and this is a function of the particular dielectric medium enveloping the solvent. The observed redshifts for quinoline are consistent with the evolution of the Lorentz−Lorenz polarizability parameter of the solvent $P = (n^2 - 1)/(n^2 + 2)$,[45,46] n being the solvent index of refraction in the 313 nm region.[47] The observations are as follows. In an argon matrix at 11 K (P = 0.181) the redshift is 88 cm^{-1},[48] ∼215 cm^{-1} in a methanol matrix at 10 K[48] (P = 0.2152), ∼190 cm^{-1} in an ethanol matrix at 93 K[49] (P = 0.2358), ∼210 cm^{-1} in a room-temperature ethanol solution[17] (P = 0.2358), ∼240 cm^{-1} in a room-temperature cyclohexane solution[16] (P = 0.2723), and ∼260 cm^{-1} in a 3-methyl pentane matrix at 77 K[50] (P = 0.284).

The structured features in the 3.6−5.4 eV energy frame are assigned to two $\pi-\pi^*$ transitions, namely, $2^1A' \leftarrow 1^1A'$, whose origin band at 3.991 eV has a calculated energy 4.09 eV[38] (f = 0.060), and the $3^1A' \leftarrow 1^1A'$ transition, whose origin we assign to the band at 4.441 eV, in reasonable agreement with the value ∼4.22 eV listed by Innes et al.[10] (see also below). We remark that, from our DFT calculations, the $1^1A'' \leftarrow 1^1A'$ n$-\pi^*$ transition is also expected in this energy region, below, but close to, the $\pi-\pi^*$ $2^1A' \leftarrow 1^1A'$ origin (Table 4). Favini et al.[16] assigned a cyclohexane solution spectrum band at 3.96 eV to n$-\pi^*$ and consider a band maximum at 4.59 eV, as do Amma et al. at 4.52 eV in the gas-phase spectrum,[13] to be due to a $\pi-\pi^*$ transition, which both groups consider (erroneously) to be the first $\pi-\pi^*$ transition $2^1A' \leftarrow 1^1A'$. According to the gas-phase observations of Hiraya et al.,[15] the very weak $1^1A'' \leftarrow 1^1A'$ n$-\pi^*$ transition occurs close to the $\pi-\pi^*$ spectral region, with a transition origin band at 30 388 cm^{-1} (3.768 eV), ∼1850 cm^{-1} below the $\pi-\pi^*$ transition. This n$-\pi$ transition is too weak to be observed in our absorption study. Indeed our DFT calculations predict the $1^1A'' \leftarrow 1^1A'$ n$-\pi^*$ transition oscillator strength to be ∼10 times weaker than that of the $2^1A' \leftarrow 1^1A'$ $\pi-\pi^*$ transition (Table 4).

In the high-resolution gas-phase spectrum of Hiraya et al.[15] the $\pi-\pi^*$ origin band is complex, indicative of near-resonance vibronic coupling between the n$-\pi^*1^1A''$ and $\pi-\pi^*$ $2^1A'$levels. Our 3.991 eV (32 190 cm^{-1}) band peak has an absorption cross-section of 8.91 Mb, and it has two companion features, one at −56 cm^{-1} (8.42 Mb) and the other at +42 cm^{-1} (8.20 Mb) (Table 5). These energy values are in excellent agreement with the corresponding features at −59 and +39 cm^{-1} from their origin band peak at 32 192 cm^{-1} that we measured from Figure 2 of the resonance-enhanced two-photon ionization spectrum of Hiraya et al.[15] The envelope of these three features in our spectrum (Figure 3) has a full width at half-maximum (fwhm) value of ∼30 meV, which is consistent with the profile of the complex origin band in the resonance-enhanced two-photon ionization spectrum and with the fwhm of the corresponding band in the Ar matrix spectrum.[48]

The other spectral features in the 3.8−4.4 eV region are mainly vibrational components of the lowest singlet−singlet $\pi-\pi^*$ transition. They have corresponding features in the condensed-phase absorption spectra,[12,13,48,50] while the published vapor-phase spectra concentrate only on the $\pi-\pi^*$

Table 5. Quinoline Gas-Phase Absorption Spectrum: Band Energies and Assignments[a]

band no.	energy, eV	energy, cm^{-1}	assignment: vibrational frequencies in cm^{-1}	quantum defect of Rydberg series O^0_0 bands
1	3.984	32 134	−56 see text	
2	3.991	32 190	$2^1A' \leftarrow 1^1A'\ O^0_0$	
3	3.996	32 232	+ 42 see text	
4	4.065 (sh)	32 788		
5	4.080	32 906	$2^1A' \leftarrow 1^1A'\ x^1_0$	
6	4.120	33 228	$2^1A' \leftarrow 1^1A'\ y^1_0$	
7	4.125	33 272	$2^1A' \leftarrow 1^1A'\ y^1_0$ + 44 see text	
8	4.163	33 573	$2^1A' \leftarrow 1^1A'\ z^1_0$	
9	4.165	33 590	$2^1A' \leftarrow 1^1A'\ x^2_0$	
10	4.250	34 282	$2^1A' \leftarrow 1^1A'\ x^1_0 z^1_0$; $2^1A' \leftarrow 1^1A'\ y^2_0$	
11	4.295	34 638	$2^1A' \leftarrow 1^1A'\ y^1_0\ z^1_0$	
12	4.343	35 026	$2^1A' \leftarrow 1^1A'\ z^2_0$; $2^1A' \leftarrow 1^1A'\ x^2_0\ z^1_0$	
13	4.441	35 819	$3^1A' \leftarrow 1^1A'\ O^0_0$	
14	4.527	36 513	$3^1A' \leftarrow 1^1A'\ x^1_0$	
15	4.630	37 343	$3^1A' \leftarrow 1^1A'\ z^1_0$	
16	4.707	37 965	maximum of broad diffuse background	
17	4.868 (sh)	39 263		
18	5.486	44 247	$4^1A' \leftarrow 1^1A'\ O^0_0$	
19	5.519	44 511	$4^1A' \leftarrow 1^1A'\ O^0_0$ + 264 (264 = a″ vib) see text)	
20	5.538	44 667	$4^1A' \leftarrow 1^1A'\ O^0_0$ + 420 (420 = (a″ vib) see text)	
21	5.586	45 054	$4^1A' \leftarrow 1^1A'\ x^1_0$	
22	5.603	45 187	$4^1A' \leftarrow 1^1A'\ y^1_0$	
23	5.669	45 724	$4^1A' \leftarrow 1^1A'\ z^1_0$	
24	5.693	45 914	$4^1A' \leftarrow 1^1A'\ x^2_0$	
25	5.724	46 168	$4^1A' \leftarrow 1^1A'\ y^2_0$	
26	5.761	46 468	$4^1A' \leftarrow 1^1A'\ x^1_0\ z^1_0$	
27	5.791	46 707	$4^1A' \leftarrow 1^1A'\ x^3_0$	
28	5.869	47 336	$4^1A' \leftarrow 1^1A'\ x^2_0\ z^1_0$	
29	5.949	47 984	R1 (n = 3) O^0_0	R1 δ = 0.746
30	6.022 (sh)	48 570	R1 (n = 3) x^1_0; R2 (n = 3) O^0_0	R2 δ = 0.715
31	6.102 (sh)	49 220	$5^1A' \leftarrow 1^1A'\ O^0_0$	
32	6.218	50 150	$6^1A' \leftarrow 1^1A'\ O^0_0$	
33	6.357 (sh)	51 272	$6^1A' \leftarrow 1^1A'\ y^1_0$	
34	6.400	51 620	$6^1A' \leftarrow 1^1A'\ x^1_0 y^1_0$	
35	6.495	52 384	$6^1A' \leftarrow 1^1A'\ y^2_0$	
36	6.538 (sh)	52 732	$6^1A' \leftarrow 1^1A'\ x^1_0 y^2_0$	
37	6.659 (sh)	53 708	$7^1A' \leftarrow 1^1A'\ O^0_0$	
38	6.792	54 781	$7^1A' \leftarrow 1^1A'\ y^1_0$	
39	6.909	55 725	$7^1A' \leftarrow 1^1A'\ y^2_0$	
40	6.981	56 306	$8\ ^1A' \leftarrow 1^1A'\ O^0_0$ broad band $\Delta E \approx$ 50 meV	
41	7.083	57 126	$8^1A' \leftarrow 1^1A'\ x^1_0$	
42	7.177	57 887	R1 (n = 4) O^0_0	R1 δ = 0.938
43	7.204 (sh)	58 105	$8^1A' \leftarrow 1^1A'\ x^2_0$	
44	7.242 (sh)	58 407	R1 (n = 4) x^1_0	
45	7.274	58 668	R1 (n = 4) y^1_0	
46	7.335	59 160	$8^1A' \leftarrow 1^1A'\ x^3_0$	
47	7.345	59 241	R1 (n = 4) z^1_0	
48	7.373	59 467	R1 (n = 4) y^2_0	
49	7.403	59 709	R2 (n = 4) O^0_0	R2 δ = 0.871
50	7.449	60 077	R1 (n = 4) $y^1_0\ z^1_0$; $8^1A' \leftarrow 1^1A'\ x^4_0$	
51	7.546	60 864	R1 (n = 4) $y^2_0\ z^1_0$	
52	7.609	61 638	R3 (n = 3) O^0_0	R3 δ = 0.876
53	7.653	61 728		
54	7.795	62 873	$12\ ^1A' \leftarrow 1^1A'\ O^0_0$	
55	7.815 (sh)	63 032		
56	7.830	63 151	R1 (n = 5) O^0_0	R1 δ = 0.871
57	7.852	63 331	$12\ ^1A' \leftarrow 1^1A'\ x^1_0$	
58	7.869 (sh)	63 467		
59	7.897	63 694	R2 (n = 5) O^0_0; R1 (n = 5) x^1_0	R2 δ = 0.685
60	7.917	63 855	$12\ ^1A' \leftarrow 1^1A'\ x^2_0$	
61	7.955	64 164	R1 (n = 5) x^2_0	
62	7.981	64 371	R1 (n = 5) z^1_0	
63	7.996	64 495		
64	8.025	64 725	R6 (n = 3) O^0_0; R1 (n = 5) x^3_0	R6 δ = 0.979
65	8.043	64 872		
66	8.075	65 126		
67	8.080	65 168	R1 (n = 6) O^0_0	R1 δ = 1.018
68	8.097	65 306		
69	8.109	65 402		
70	8.125	65 531		
71	8.149	65 726	R2 (n = 6) O^0_0; R1 (n = 6) x^1_0	R2 δ = 0.670
72	8.177	65 952	R4 (n = 3) O^0_0; R1 (n = 6) y^1_0	R4 δ = 0.642
73	8.192	66 072		
74	8.208	66 203		
75	8.246	66 511	R1 (n = 7) O^0_0	R1 δ = 1.029
76	8.263	66 644		
77	8.285	66 822	R2 (n = 7) O^0_0	R2 δ = 0.670
78	8.304	66 979		
79	8.335	67 227		
80	8.346	67 317	R1 (n = 8) O^0; R1 (n = 7) y^1_0	R1 δ = 1.050
81	8.360	67 431		
82	8.414	67 866	R1 (n = 9) O^0_0	R1 δ = 1.021
83	8.423	67 936		
84	8.440	68 073	R1 (n = 8) y^1_0	
85	8.460	68 236	R1 (n = 10) O^0_0	R1 δ = 0.995
86	8.492	68 493	R1 (n = 11) O^0_0	R1 δ = 0.994
87	8.515	68 681	R1 (n = 12) O^0_0	R1 δ = 1.008
88	8.530	68 799	R1 (n = 13) O^0_0	R1 δ = 1.217
89	8.548	68 944	R1 (n = 14) O^0_0	R1 δ = 0.983
90	8.560	69 037	R1 (n = 15) O^0_0	R1 δ = 0.907
91	8.568	69 108	R1 (n = 16) O^0_0	R1 δ = 0.891
92	8.583	69 228		
93	8.607	69 420		
94	8.616	69 492		
95	8.631	69 613		
96	8.652	69 784		
97	8.689	70 081		
98	8.741	70 497	R7 (n = 3) O^0_0	R7 δ = 0.719
99	8.803	70 997	R7 (n = 3) x^1_0	
100	8.840	71 301	R5 (n = 3) O^0_0	R5 δ = 0.239
101	8.913	71 890		
102	9.147	73 774	R3 (n = 4) O^0_0	R3 δ = 0.966
103	9.273	74 794		
104	9.340	75 329		
105	9.414 (sh)	75 929	R4 (n = 4) O^0_0	R4 δ = 0.645

Table 5. continued

band no.	energy, eV	energy, cm^{-1}	assignment: vibrational frequencies in cm^{-1}	quantum defect of Rydberg series O^0_0 bands
106	9.468 (sh)	76 374		
107	9.563 (sh)	77 130		
108	9.619	77 579	R5 (n = 4) O^0_0	R5 δ = 0.319
109	9.679	78 064	R8 (n = 3) O^0_0	R8 δ = 0.151
110	9.717	78 369		
111	9.7779	78 864	R3 (n = 5) O^0_0	R3 δ = 0.992
112	9.8400	79 365	R6 (n = 4) O^0_0; R3 (n = 5) x^1_0	R6 δ = 1.003
113	9.9068	79 903	R4 (n = 5) O^0_0; R6 (n = 4) x^1_0	R4 δ = 0.642
114	10.0108	80 742	R5 (n = 5) O^0_0	R5 δ = 0.286
115	10.0637 (sh)	81 169	R5 (n = 5) x^1_0	
116	10.0759	81 267	R3 (n = 6) O^0_0	R3 δ = 1.022
117	10.0882	81 366	R7 (n = 4) O^0_0	R7 δ = 0.723
118	10.1419	81 799	R4 (n = 6) O^0_0; R7 (n = 4) x^1_0	R4 δ = 0.682
119	10.2087	82 338	R5 (n = 6) O^0_0	R5 δ = 0.269
120	10.2466	82 644	R3 (n = 7) O^0_0	R3 δ = 1.004
121	10.2593 (sh)	82 736		
122	10.313 (sh)	83 180	R5 (n = 7) O^0_0; R3 (n = 7) x^1_0	R5 δ = 0.375
123	10.3449	83 437	R3 (n = 8) O^0_0	R3 δ = 1.030
124	10.375	83 680		
125	10.3970	83 857	R8 (n = 4) O^0_0; R5 (n = 8) O^0_0	R8 δ = 0.231; R5 δ = 0.241
126	10.408	83 946	R3 (n = 9) O^0_0	R3 δ = 1.080
127	10.4452	84 246		
128	10.4894	84 602		
129	10.5116	84 781	R6 (n = 5) O^0_0	R6 δ = 0.984
130	10.532 (sh)	84 946		
131	10.5698	85 251	R6 (n = 5) x^1_0	
132	10.5924	85 433		
133	10.6060	85 543	R7 (n = 5) O^0_0	R7 δ = 0.738
134	10.6196	85 652		
135	10.6379	85 780		
136	10.6470	85 873		
137	10.6561	85 947	R7 (n = 5) x^1_0	

[a]sh = shoulder. Vibrational modes x, y, and z are specific to the various $m^1A' \leftarrow 1^1A'$ valence transitions and to the Rydberg transitions.

Table 6. Quinoline $\pi-\pi^*$ $m^1A' \leftarrow 1^1A'$ Singlet Transitions: Calculated Energies (eV) and Oscillator Strengths

A′state	Fav[17]	Mat[43]	Tin[40]	Nish[39]	Baba[38]	Rid[41]	Wag[42]	DFT present study	observed transition energy	DFT -obs unsigned (UD)	Baba−obs unsigned (UD)
2 ^1L_a		4.231	4.00 0.026	3.97 0.052	4.09 0.060	4.14 0.04	4.07 0.04	4.6484 0.0274	3.991	0.657	0.10
3 ^1L_b	4.42 0.076	4.270	4.527 0.163	4.47 0.170	4.32 0.207	4.54 0.16	4.86 0.19	4.7312 0.0622	4.441	0.29	0.12
4 ^1B_b	5.546 0.005	5.813	5.460 0.753	5.29 0.583	5.43 0.353	5.47 0.67		6.0226 0.9655	5.486	0.537	0.06
5			5.786 1.077	5.64 0.194	5.61 0.201		5.78 0.15	6.2419 0.0489	6.102	0.14	0.49
6			5.883 0.196	5.88 0.187	5.91 0.165	5.84 0.02		6.4344 0.1934	6.218	0.217	0.31
7			6.146 0.513	5.78 1.034	6.04 1.272	5.94 1.15		6.5980 0.2540	6.659	0.061	0.62
8			6.229 0.149	6.17 0.691	6.33 0.764	6.15 0.57		6.8529 0.1008	6.981	0.128	0.65
9				6.95 0.002	7.11 0.003	6.72 0.15		7.2399 0.0378			
10								7.5841 0.0006			
11								7.7013 0.0035			
12								7.8613 0.0464	7.795	0.066	
13								7.9459 0.0085			
14								7.9979 0.0016			

origin band. An exception is an early photographic plate spectrum reported by Amma et al.[13] in which the $\pi-\pi^*$ transition features are observed at higher resolution and, as mentioned above, erroneously assigned to the n−π^* transition.

We assign band number 5 at 4.080 eV to the vibronic transition $2^1A' \leftarrow 1^1A'$ x^1_0, where the x vibrational mode of quinoline has a frequency of the order $\nu(x) \approx 710$ cm^{-1}. This is probably a C−H bend mode, whose ground-state frequency of 741 cm^{-1} is characteristic of the presence of four neighboring hydrogen atoms in quinoline.[51] Amma et al.[13] report the analogous x^1_0 band in their vapor-phase spectrum at $\Delta\nu$ = 707 cm^{-1} from their reputed origin band, whereas in the absorption spectrum of quinoline in an Ar matrix at 11 K of Crépin et al.,[48] we determine from their Figure 3 a value of $\Delta\nu \approx 725$ cm^{-1}. The corresponding value in a 3MP solvent at 77 K is $\Delta\nu \approx 690$ cm^{-1} that we obtained from Figure 2 of the study by Anton and Moomaw.[50]

A number of other vibronic features of the $2^1A' \leftarrow 1^1A'$ transition were assigned to band nos. 5−12. These involve excitation of two other vibrational modes, namely, $\nu(y) \approx 1050$ cm^{-1} and $\nu(z) \approx 1400$ cm^{-1}. The $\nu(z)$ frequency is in the region characteristic of C═C and C═N stretching vibrations in the quinoline ground state.[52] Band no. 7 occurs at 44 cm^{-1} beyond the $2^1A' \leftarrow 1^1A'$ y^1_0 vibronic transition (Band no. 6) and so may be related to the +42 cm^{-1} component (Band no. 3) of the complex origin region.

We return now to the question of the energy of the second $\pi-\pi^*$ valence transition $3^1A' \leftarrow 1^1A'$, whose origin we assign to band no. 13 at 4.441 eV. The MO calculations of Baba and Yamazaki place $3^1A' \leftarrow 1^1A'$ transition at 4.32 eV, f = 0.123,[38] while Nishimoto[39] calculates 4.527 eV, f = 0.163 (Table 6). Wagner et al.[42] calculate this transition at 4.86 eV (f = 0.19) and consider it to correspond to the ^1L_a (short axis polarized) transition in the nomenclature of Platt, based on his free electron model.[53]

The ^1L_a assignment was also made by Zimmerman and Joop[49] on the basis of fluorescence polarization measurements. These authors state that, from their spectra of quinoline in ethanol solution, it is not possible to determine the precise energy of the ^1L_a state origin, because it lies within the extensive ^1L_b band region (Platt notation), that is, the $2^1A' \leftarrow 1^1A'$ transition region in our nomenclature. However, they do note that there is a marked minimum in the polarization spectrum at ~4.35 eV, where one might expect to find the origin region of the ^1L_a transition, in reasonable agreement with our assignment. We note also that, in magnetic circular dichroism (MCD) studies of quinoline in *n*-heptane solution by Kaito and Hitano[54] and by Vašák et al.[55] in cyclohexane solution, the $3^1A' \leftarrow 1^1A'$ origin is considered to be at ~36 000 cm^{-1} (4.46 eV), where there is a minimum in the MCD curve.

The experimental and theoretical results discussed above are consistent with our assignment of the O^0_0 origin of the $3^1A' \leftarrow 1^1A'$ transition to Band no. 13 at 4.441 eV. This occurs at the initial rising part of a broad continuous background 4.3−5.2 eV, discussed below. Band nos. 14 and 15 are assigned to vibronic components of the $3^1A' \leftarrow 1^1A'$ valence transition, involving $\nu(x) \approx 700$ cm^{-1} and $\nu(z) \approx 1480$ cm^{-1}. The $\nu(x)$ frequency is probably that of a C−H bend mode, as in the case of a similar vibronic component of the $2^1A' \leftarrow 1^1A'$ transition. No other vibrations appear to be excited in the $3^1A' \leftarrow 1^1A'$ electronic transition.

We note that the series of band nos. 2−15 assigned to vibronic components of the first two $\pi-\pi^*$ valence transitions are observed with various degrees of spectral resolution in several condensed-phase absorption spectra.[17,48−50] In view of possible differential solvent shift effects and also effects on vibronic levels due to vibronic interactions between the $n-\pi^*$ and $\pi-\pi^*$ states,[16] exact correspondence between vapor-phase and condensed-phase vibrational intervals is not to be expected. Apart from the rarity of reported band energies in published condensed-phase spectra of quinoline, the resolution of our spectra is insufficient to further pursue these possible influences of solvent or matrix on quinoline vibronic level energies, apart from that on the origin band of the ^1L_b transition, discussed above.

The 3.9−4.630 eV featured bands overlie a broad diffuse band up to ~5.15 eV (Figures 2 and 3), whose maximum intensity, at 4.707 eV (band no. 16), has an absorption cross section of 11.43 Mb. The absorption spectrum of quinoline in a 3MP matrix at 77 K in the 3.8−4.9 eV region[50] is very similar in features to our gas-phase absorption spectrum in this same spectral region, and it exhibits a broad band whose maximum is at ~4.6 eV.

It is not immediately clear how to assign the broad 4.707 eV band. One possibility would be to reinterpret the 3.8−4.4 eV region features as all belonging to the lowest $n-\pi^*$ transition $1^1A'' \leftarrow 1^1A'$ and assign the broad 4.4−5.15 eV band to the $\pi-\pi^*$ transition $2^1A' \leftarrow 1^1A'$. However, the work of Hiraya et al.,[15] who clearly identified the location of the $1^1A'' \leftarrow 1^1A$ $n-\pi^*$ transition, rules this out. A more reasonable assignment is that the broad diffuse band is related in some way to the second $\pi-\pi^*$ transition $3^1A' \leftarrow 1^1A'$, the ^1L_a band. We note that the profile of this band region is similar to that of the corresponding band in solution absorption spectra of naphthalene, although the latter exhibits more pronounced overlying vibrational features[17] than does quinoline. The diffuse character of the quinoline band in the 4.7 eV region is perhaps a sign of extensive rovibronic interactions of the $3^1A'$ electronic state with a high density of rovibronic levels of lower-lying electronic states. Fluorescence excitation spectra of quinoline provide some support for the existence of these interactions, which can lead to the observed diminished fluorescence quantum yield in the excitation region of this broad diffuse absorption feature.[14,50]

III.1.2. Valence Transitions: 5.4−7.5 eV. Transitions to the $4^1A'$ and Higher-Energy Electronic States. The absorption spectrum of quinoline is structured in the 5.4−7.5 eV region (Figures 2 and 4−6). A group of bands starting at 5.486 eV

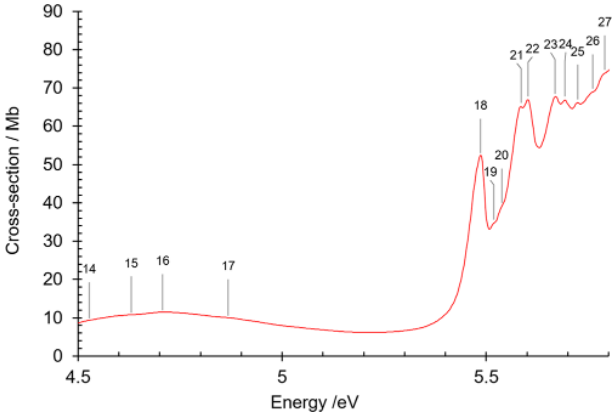

Figure 4. Quinoline absorption spectrum 4.5−5.8 eV. Band numbers are pinpointed.

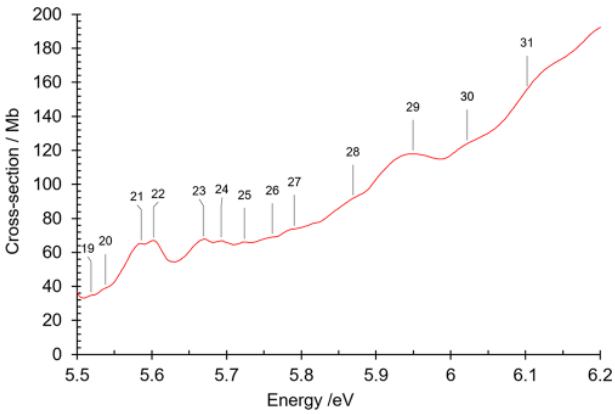

Figure 5. Quinoline absorption spectrum 5.5−6.2 eV. Band numbers are pinpointed.

(Bands 18−28) overlies a broad band that continues up to ~6.8 eV. It contains some bands mainly as shoulders, the principal features being small peaks at 5.761 and 5.949 eV and shoulders at 6.022 and 6.102 eV (Table 5, Figures 2 and 5). The absorption rises to a maximum at 6.218 eV with a cross section of 193.6 Mb. On the high-energy side of this broad band there are several somewhat diffuse features (Band nos. 33−37).

A few of the structured features in the 5.4−5.8 eV region are also observed in solution spectra, whose upper limit is generally ~5.7 eV,[16,17,49,54,55] and are therefore are unlikely to be Rydberg bands, since these are almost never observed in solution spectra except as much broadened bands.[56] We assign band nos. 18−28 between 5.486 and 5.869 eV to the ^1B_b band (Platt notation[53]), in agreement with some previous studies,[17]

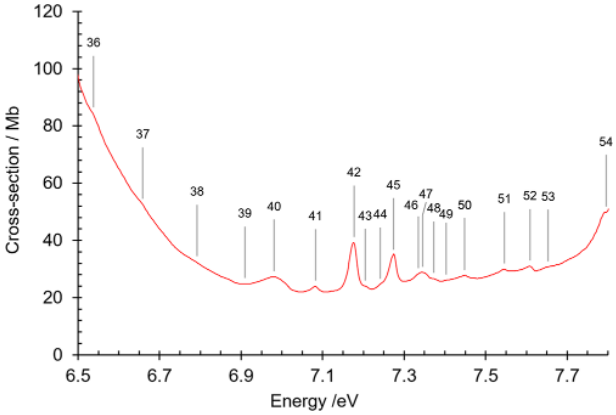

Figure 6. Quinoline absorption spectrum 6.5−7.8 eV. Band numbers are pinpointed.

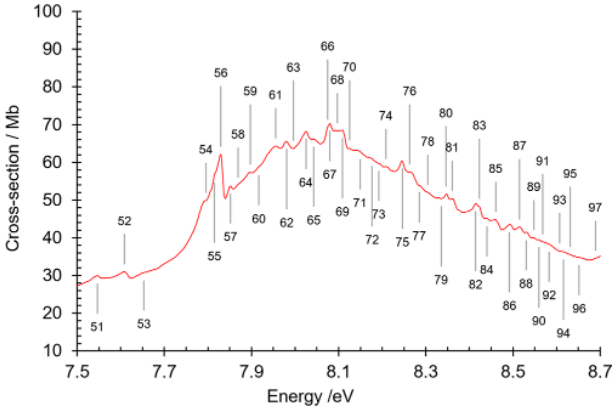

Figure 7. Quinoline absorption spectrum 7.5−8.7 eV. Band numbers are pinpointed.

that is, to the $4^1A' \leftarrow 1^1A'$ $\pi-\pi^*$ transition. The O^0_0 transition origin is band no. 18 at 5.486 eV and is red-shifted in solution by several hundred inverse centimeters,[16,17,49] in line with the solvent polarizability parameter discussed above.

The $4^1A' \leftarrow 1^1A'$ transition vibronic components, assigned in band nos. 18−28, include excitation of two low-frequency vibrations, of frequencies ~270 cm^{-1} (band no. 19) and ~410 cm^{-1} (band no. 20), that are undoubtedly of a″ symmetry (allowed in a dipole transition of a C_s symmetry molecule). Other vibronic components of this transition are assigned to three vibrational modes $\nu(x) \approx 820$ cm^{-1}, $\nu(y) \approx 950$ cm^{-1}, and $\nu(z) \approx 1450$ cm^{-1}.

The broad diffuse band whose maximum is at ~6.218 eV overlies the minor features at 5.949 and 6.102 eV. The $\pi-\pi^*$ $5^1A' \leftarrow 1^1A'$, $6^1A' \leftarrow 1^1A'$, $7^1A' \leftarrow 1^1A'$, and $8^1A' \leftarrow 1^1A'$ transitions are expected to occur in this region (Table 6). Molecular orbital calculations by Baba and Yamazaki[38] predict $\pi-\pi^*$ transitions at 5.61 eV ($f = 0.201$), 5.91 eV ($f = 0.165$), 6.04 eV ($f = 1.272$), and 6.33 eV ($f = 0.764$). Thus, we expect several valence transitions to be observed in this spectral region.

However, this is also a region where we observe Rydberg bands. The 5.949 eV feature (band no. 29) is assigned as the origin band of the $n = 3$ member of the R1 Ry series, discussed in Section III.1.3 below. We note that the band nos. 18−28 that are vibronic components of the $4^1A' \leftarrow 1^1A'$ electronic transition (Table 5) remain reasonably sharp but are red-shifted by 65 cm^{-1} in *n*-heptane solution according to our measurements of Figure 1 of the publication of Kaito and Hatano,[54] while the band no. 29 at 5.949 eV has a red shift of 150 cm^{-1} and is considerably broadened in *n*-heptane solution. This is consistent with band no. 29 being an $n = 3$ Ry band.

Furthermore, in the *n*-heptane solution absorption spectrum[54] the broad band maximum is found at 6.06 eV, red-shifted by ~1270 cm^{-1} with respect to the gas-phase value of 6.218 eV (band no. 32). In the pure liquid phase of quinoline studied by MacRae et al.,[18] our measurements of their Figure 7 show that the $2^1A' \leftarrow 1^1A'$ transition vibronic features remain reasonably sharp, while the $4^1A' \leftarrow 1^1A'$ transition features are completely smoothed out, forming a broad feature whose maximum is at ~5.41 eV. This broadening could be due to valence-Rydberg state interactions in this energy region. The broad band 5.8−6.9 eV that we assign as background to the three $\pi-\pi^*$ valence transitions $5^1A' \leftarrow 1^1A'$, $6^1A' \leftarrow 1^1A'$, and $7^1A' \leftarrow 1^1A'$ (Table 5), discussed below, has a maximum at ~5.92 eV in the pure liquid phase, thus being red-shifted by ~2400 cm^{-1} (300 meV) with respect to the gas phase.

The 6.102 eV feature in our gas-phase absorption spectrum is assigned as the origin band of the $5^1A' \leftarrow 1^1A'$ valence transition, while the peak at 6.218 eV is considered to be the origin of the $6^1A' \leftarrow 1^1A'$ transition. These two transitions are generally calculated to have an oscillator strength of $f \approx 0.2$ but are not the strongest calculated valence transitions (Table 6). The high absorption cross-section in the 6.218 eV region (193.6 Mb) must therefore be due in part to plasmon-type effects, that is, to collective modes of the π electrons that could contribute to strong absorption in the 6 eV region.[57−60] These collective oscillations (plasmon-type) are many-body effects and are not dealt with in Hartree−Fock single-particle calculations. The related molecule naphthalene has a strong absorption peak at 5.89 eV[61] that has been interpreted as plasmon-type,[60] reinforcing the ^1B_b $\pi-\pi^*$ valence transition intensity.[62]

Vibrational components of the $5^1A' \leftarrow 1^1A'$ transition, if they exist, are apparently hidden in the broad background absorption. The $6^1A' \leftarrow 1^1A'$ valence transition has two vibrational components, with frequencies $\nu(x) \approx 350$ cm^{-1} and $\nu(y) \approx 1120$ cm^{-1} appearing in bands $6^1A' \leftarrow 1^1A'$ y^1_0; $x^1_0\,y^1_0$; y^2_0 and $x^1_0\,y^2_0$ (Table 5). The one-quantum band x^1_0 that would be expected at ~6.261 eV is probably hidden in the intense background continuum close to the 6.218 eV maximum.

The origin of the $7^1A' \leftarrow 1^1A'$ transition is assigned to band no. 37 at 6.659 eV. It is expected to be a strong transition (Table 6). The absorption cross-section at that energy, enhanced by the important plasmon-type background mentioned above, is 52 Mb. This electronic transition has two vibronic components y^1_0 and y^2_0, where $\nu(y) \approx 1050$ cm^{-1}.

The origin band of the $8^1A' \leftarrow 1^1A'$ $\pi-\pi^*$ transition is taken as the broad feature whose maximum is at 6.981 eV (band no. 40). It has an fwhm of ~50 meV and thus probably contains unresolved substructure. Its breadth thus makes it difficult to pinpoint an exact origin band frequency. A four-member vibrational progression in $\nu(x) \approx 900$ cm^{-1} forms the vibronic components. The $8^1A' \leftarrow 1^1A'$ $\pi-\pi^*$ transition was predicted by several calculations to be in the region of 6.2 ± 0.1 eV (Table 6). Our DFT calculation value of 6.853 eV is much closer to the experimental assignment.

We also assigned a few vibronic bands as belonging to the $12^1A' \leftarrow 1^1A'$ transition, with an origin at 7.795 eV, predicted by the DFT calculations at 7.861 eV to be the strongest of the higher-energy valence transitions. Indeed, these calculations predict a series of mainly weak higher-energy $\pi-\pi^*$ valence transitions $9^1A' \leftarrow 1^1A'$ to $14^1A' \leftarrow 1^1A'$ over a restricted energy range of 7.58−8 eV. The $9^1A' \leftarrow 1^1A'$, $10^1A' \leftarrow 1^1A'$, and $11^1A' \leftarrow 1^1A'$ transitions, DFT calculated to be in the 7.24−7.7 eV region, may be present unresolved among the broad features between 7.3 and 7.7 eV (Figure 6).

III.1.3. A Comment on the Valence-Transition Calculations. In Table 6, where we compare the calculated and observed transition energies of quinoline, we note that the unsigned difference (UD) between the DFT-calculated energies and our assigned spectral energies ranges from 0.06 to 0.66 eV, the average over the eight $\pi-\pi^*$ transitions being 0.26 eV. There have been several TD-DFT calculations of the electronic state energies of benchmark test diatomic and polyatomic molecules,[20,63−73] mainly limited to singlet valence excited states, but some have included triplet and Rydberg states. Most of these studies set out to compare the efficiencies of various functionals, among which the hybrid density functional B3LYP, with its 20% of Hartree−Fock exchange in the functional,[73] is one of the best. One typical criterion of the quality of TD-DFT calculation performance is as follows: when mean unsigned errors (MUE, where UE is equivalent to our UD) in calculated excited electronic state energies are less than 0.36 eV the TD-DFT calculations are considered to be "successful",[73] the range of actual UE values in a typical set of benchmark molecules being quite large, up to and greater than 1 eV. The results of our TD-TFT calculations on quinoline are thus perfectly in line with the results of benchmark calculations.[63−73] However, our calculated energies, as are the benchmark test cases, are very far from "spectroscopic accuracy" or even the 0.05 eV of "chemical accuracy". Possible sources of errors in TD-DFT calculations are discussed by Burke et al.,[37] in particular, the adequacy of the means used to take into account the exchange-correlation potential and the associated possibility of breakdown of the local adiabatic approximation that is relevant to frequency-independent exchange-correlation functionals with which the exchange-correlation potential adjusts instantaneously to changes in the electron density. We can add to this the problem of the adequacy of the chosen basis set. Various sources of error in TD-DFT calculations of the excited-state energies of acenes have been discussed in detail by Grimme and Parac,[74] and for heteroaromatic molecules by Prilj et al.,[75] in particular, the sensitivity of L_b states to correlation effects, while L_a states have significant double excitation character.

In Table 6 we also list the UD values for the difference between the observed and the $\pi-\pi^*$ excitation energies calculated by Baba and Yamazaki[38] by the Pariser−Parr−Pople SCF LCAO MO method plus the inclusion of configuration interaction. These have the lowest set of UD values among the various calculation studies listed in Table 6. The range of the Baba and Yamazaki UD values is from 0.06 to 0.65 eV, and the average value is 0.34 eV, ∼30% greater than for our DFT calculation. It is of interest that there is a trend to smaller UD values with increasing excitation energy in our DFT calculation, while the trend is to larger UD values in the P−P−P calculation of Baba and Yamazaki.

III.1.4. Rydberg and Other Transitions: 7.1−10.7 eV. There are no previous observations of Rydberg bands in quinoline. We assigned many of the bands observed between 7.1 and 10.7 eV to several Rydberg series that converge to various electronic states of the ion (Figure 8). We first discuss the energies of the ion states.

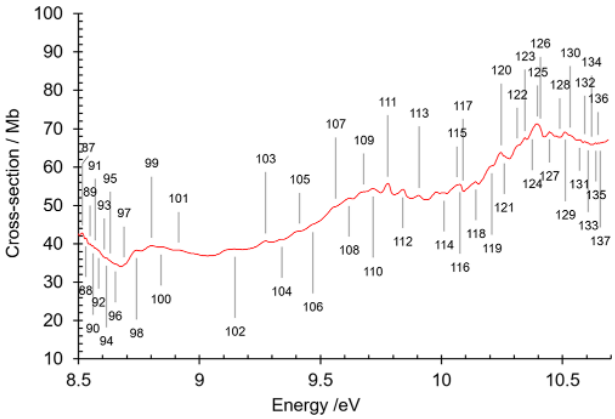

Figure 8. Quinoline absorption spectrum 8.5−10.7 eV. Band numbers are pinpointed.

The initial ionization energy of quinoline has been measured mainly by He I photoelectron spectroscopy. Reported values are 8.67 eV,[76] 8.62 eV,[27,77−79] 8.65 eV,[77] 8.61 ± 0.02 eV,[80] as well as ion yield curve onset values of 8.62 ± 0.01 eV[81] and 8.57 ± 0.05 eV.[82] Reported successive ionization energies are 9.18, 9.39, 10.57, 11.3, 11.5, 11.9, and 12.4 eV.[27,78,83] We will refer to the ground doublet electronic state of quinoline as D_0 and to the successive excited states as D_1-D_7.

As a result of our observation of an extensive R1 series of Rydberg bands, from $n = 3$ to $n = 16$, converging on the ion ground state, we were able to refine the value of the ionization energy. In establishing the R1 series (see below) we explored the following trial ionization energies (IEs) over the range of IE = 8.620−8.630 eV at intervals of 0.0025 eV. On the basis of the simple assumption, usually made,[84] that the quantum defect δ is approximately constant for a given progression in n, we found that the most consistent set of δ values over the whole series was obtained with IE = 8.628 eV. We adopted this as the adiabatic ionization energy of quinoline to the D_0 ground state.

Determination of the ionization energies to the excited ion states was accomplished using transition energy data from the electronic spectra of gas-phase quinoline-Ar complexes observed by Dryza et al.[83] They were able to estimate the $D_3 \leftarrow D_0$ and $D_4 \leftarrow D_0$ electronic transition energies of the bare ion as 1.995 and 2.2727 eV, respectively. On the basis of DFT calculations they also predicted the $D_1 \leftarrow D_0$ and $D_2 \leftarrow D_0$ transition energies to be 0.718 and 0.916 eV, respectively.

Using this information, we list the first five ionization energies of quinoline as 8.628 eV (D_0); (9.346 eV), 9.16 eV,[78] (D_1); 9.25 ± 0.05 eV,[78] (9.544 eV) (D_2); 10.623 eV (D_3), and 11.355 eV (D_4), the D_1 and D_2 values (in brackets) being based on DFT calculations. The D_0, D_1, D_3, and D_4 levels arise, respectively, from $(HOMO)\pi^{-1}$, $(HOMO-1)\pi^{-1}$, $(HOMO-3)\pi^{-1}$, and $(HOMO-4)\pi^{-1}$ electron ejections, while the D_2 level is formed by electron ejection from $(HOMO-2)n^{-1}$, this lone pair orbital n being of σ-type (HOMO = highest occupied molecular orbital).[78]

The R1 Ry series converges on the D_0 doublet ground state of the quinoline cation (Table 5, Figure 2). Our analysis is based on the equation for the energy $E(n)$ of the nth member of a Rydberg series: $E(n) = \text{IE} - R/(n - \delta)^2$, where IE (quinoline) = 8.628 eV, R = 13.606 eV is the Rydberg constant, and δ is the quantum defect. The first members of the R1 series are n = 3 and are assigned, respectively, to band no. 29 (R1 n = 3, δ = 0.746), which occurs in a spectral region dominated by $\pi-\pi^*$ valence transitions. The succeeding members n = 4,5,6,... (Table 5) have higher quantum defects, of the order of $\delta = 1.0 \pm 0.1$. This difference in quantum defect values with respect to n = 3 is understandable in that in the n = 3 Ry state the radius of the Rydberg orbital is similar to that of the ion core, leading to some coupling with the π orbitals and resulting in deviations from the H atom model that lies behind the formula for $E(n)$. A similar difference between quantum defects for n = 3 and $n \geq 4$ Ry levels is observed for naphthalene, the hydrocarbon parent of quinoline. For naphthalene, the n = 3 members of the lowest observed Rydberg series have values $\delta \approx 0.68$,[85] while for $n \geq 4$ Ry levels the quantum defects $\delta \approx 0.85$.[61]

Members of the R1 series were assigned up to n = 16, close to the ionization limit. The limited band resolution is probably responsible for the spread of quantum defect values around $\delta \approx 1$ for the highest n values of the series. The lower value $\delta \approx 0.871$ for n = 5 may be due to interactions with the $12^1A'$ valence state in this energy region. The generally smaller quantum defect values for the lower members of a Rydberg series result from a greater effect of the core potential as compared with the higher n values. From the overall values of the quantum defect we assign the R1 Ry series as a nanosecond series arising from ejection of an electron from the HOMO π^{-1} orbital (Table 7).

Table 7. Quinoline: Rydberg Series

Rydberg series label	ion state limit	n members	quantum defect δ	Rydberg transition
R1	D_0 8.628 eV	n = 3–16	$\delta \approx 1.0$	$1^1A' \rightarrow (\text{HOMO})\pi^{-1}\text{ns}$
R2	D_0 8.628 eV	n = 3–7	$\delta \approx 0.67$	$1^1A' \rightarrow (\text{HOMO})\pi^{-1}\text{np}_1$
R3	D_3 10.623 eV	n = 3–9	$\delta \approx 0.98$	$1^1A' \rightarrow (\text{HOMO}-3)\pi^{-1}\text{ns}$
R4	D_3 10.623 eV	n = 3–6	$\delta \approx 0.66$	$1^1A' \rightarrow (\text{HOMO}-3)\pi^{-1}\text{np}_1$
R5	D_3 10.623 eV	n = 3–8	$\delta \approx 0.28$	$1^1A' \rightarrow (\text{HOMO}-3)\pi^{-1}\text{np}_2$
R6	D_4 11.355 eV	n = 3–5	$\delta \approx 0.98$	$1^1A' \rightarrow (\text{HOMO}-4)\pi^{-1}\text{ns}$
R7	D_4 11.355 eV	n = 3–5	$\delta \approx 0.72$	$1^1A' \rightarrow (\text{HOMO}-4)\pi^{-1}\text{np}_1$
R8	D_4 11.355 eV	n = 3–(5)	$\delta \approx 0.25$	$1^1A' \rightarrow (\text{HOMO}-4)\pi^{-1}\text{np}_2$

This Rydberg series has vibrational components (Table 5). These involve $\nu(x)$ 540 ± 40 cm^{-1}, $\nu(y)$ 800 ± 30 cm^{-1}, and $\nu(z) \approx$ 1300 cm^{-1}. The $\nu(x) \approx$ 540 cm^{-1} mode is probably related to the $\nu(29)$ = 522 cm^{-1} ring deformation mode of neutral ground-state quinoline (Table 2). The infrared multiphoton dissociation (IRMPD) spectrum of the quinoline ion ground state, measured in the 600–1600 cm^{-1} region,[86] has a strong broad band with two components at 700–900 cm^{-1} and other overlapping broad strong bands centered at 1170 and 1450 cm^{-1}. These are the regions of our $\nu(y) \approx$ 800 cm^{-1} and $\nu(z) \approx$ 1300 cm^{-1} R1 series vibrational components. We also note that, in the HeI photoelectron spectrum of quinoline, the first band (first ionization) has a relatively broad vibrational component whose frequency is of the order of 1300 cm^{-1}.[27] It is reasonable to consider that $\nu(y) \approx$ 800 cm^{-1} and $\nu(z) \approx$ 1300 cm^{-1} correspond, respectively, to $\nu(27)$ = 760 cm^{-1} and $\nu(14)$ = 1392 cm^{-1} in the neutral ground state, respectively, ring deformation and C–C stretch modes.

A second set of Rydberg bands converging to the ion ground state D_0 at 8.628 eV was observed for n = 3–7 levels, with quantum defect $\delta \approx 0.67$ (Table 5, Figure 2). No vibrational components were observed for this R2 series. This Rydberg series, which also arises from ejection of an electron from the HOMO π^{-1} orbital, was assigned as an np series (Table 7).

The strong underlying $\pi-\pi^*$ transition continuum in the 8 eV region (Figure 7) has an intensity maximum at ~8.1 eV (σ_{abs} = 65 Mb) that reaches a minimum at 8.66 eV, just above the IE = 8.628 eV value that we adopted as the ionization energy of quinoline. The absorption curve then develops another small broad continuum that rises to a maximum at 8.81 eV (σ_{abs} = 39 Mb) and a minimum at ~9.1 eV, followed by a rise to a maximum at 9.77 eV (σ_{abs} = 52 Mb). The minimum at 8.66 eV reflects the onset of the first ionization of quinoline, while the 9.1 eV minimum reflects the onset of higher-energy ionization channels whose reported energies are IE(D_1) = 9.16 eV and IE(D_2) = 9.25 ± 0.05 eV,[78] discussed above. Attempts to find corresponding Rydberg series converging to the D_1 and D_2 electronic states were unsuccessful.

We were able to assign three Rydberg series of bands that converge to the D_3 excited state of the quinoline ion at 10.623 eV. Bands n = 3–9 of the R3 series are listed in Table 5. They are weaker than those of the corresponding n term bands of the R1 series. The quantum defects in the R3 series are $\delta \approx 0.98$, so that we assign this series as ns-type, arising from ejection of an electron from the HOMO-3 orbital (Table 7). No vibrational components were recognized and indeed were not expected, judging from the profile of the HeI photoelectron spectrum in this ion state region[78] (see also below).

The second set of Rydberg bands converging to the D_3 ion state is limited to four O^0_0 members n = 3–6 of the R4 series (Table 5). The quantum defect is $\delta \approx 0.66$, typical of an np_1-type series (Table 7). The third series R5 has six components, n = 3–8, with a quantum defect $\delta \approx 0.28$, indicating that it is np_2-type (Table 7).

Some of the peaks in the 8–10.7 eV region (Figure 8) could be assigned to three further Rydberg series R6, R7, and R8 that converge to the D_4 excited electronic state of the cation at 11.355 eV (Table 5, Figure 2), which is formed by ejection of an electron from the HOMO-4 orbital. The series R6 consists of three assigned members, n = 3–5. The quantum defects of these bands are $\delta \approx 0.98$, with the series assigned as ns-type. The R7 Ry series (Table 5, Figure 2) has three assigned members, n = 3–5, $\delta \approx 0.72$, while the R8 series has two members, n = 3, 4, with quantum defects $\delta \approx 0.25$. Higher members of these last two fragmentary series, respectively considered as being of np_1-type and np_2-type (Table 7), are required to verify the assignments, but their Rydberg levels n > 5 are estimated to be beyond our 10.7 eV energy measurement limit.

We remark that the $D_3 \leftarrow D_0$ electronic transition of the quinoline cation, observed by absorption spectra using photodissociation spectroscopy,[83] contains a number of well-

resolved vibrational components; the weaker $D_4 \leftarrow D_0$ transition appears to be limited to the $O^0{}_0$ band. We would expect Rydberg vibrational components to mimic those in direct photoionization to the cation electronic levels. This is not necessarily the case for the cation transition vibrational components because of a possible difference in the Franck−Condon factors operative in the cation absorption transition and in the process of photoionization of the neutral molecule. Indeed, in the successive members of our quinoline Rydberg series that converge to the D_3 excited state of the ion we did not observe consistent consecutive features that could correspond to the vibrational components occurring in the cation absorption spectra. A comparison of the Dryza et al. cation spectra of quinoline[83] with HeI photoelectron spectral bands involving ionization to the D_3 excited states of the cations[76,78] appears to support the existence of a difference in the relevant Franck−Condon factors. A similar situation holds for the analogous relevant spectra of naphthalene.[61,76,78,83,87] However, higher-resolution PES spectra and/or calculation of the respective Franck−Condon factors are required to fully justify this interpretation.

The features between 9.0 and 10.7 eV overlie an important background continuum that reaches a quasi-constant cross section $\sigma_{abs} \approx 52$ Mb between 9.7 and 10.1 eV and then rises to another quasi constant cross section $\sigma_{abs} \approx 70$ Mb between 10.38 and 10.7 eV, the high-energy end of the measured absorption spectrum. The origin of the background continua requires further theoretical and experimental investigation. We remark that other valence transitions, such as $\pi-\sigma^*$, $\sigma-\pi^*$, and $\sigma-\sigma^*$, could be active besides the known $\pi-\pi^*$ and $n-\pi^*$ transitions and be responsible for an intense background that interferes little with the Rydberg and valence states.

We also examined whether some of the small peaks in the 9.77 to 11 eV region could be due to Rydberg transitions of a water impurity. However, we rejected this water conjecture after careful comparison of our spectrum with published absorption spectra and assignments of H_2O in this spectral region.[88−92] We were also assured that the same spectral features in the 9.77−11 eV region are not due to noise by the fact that they are exactly reproduced in a series of successive VUV absorption runs.

III.1.5. Comparison with the Absorption Spectrum of Liquid Quinoline. It is of interest to examine the absorption spectrum of liquid quinoline in the VUV region and to compare it with our gas-phase observations. MacRae et al.[18] studied the optical properties of liquid quinoline by reflectance and transmission measurements in the 2−10.6 eV spectral region. They determined absorption cross sections over the 3.5−10.6 eV range and compared their spectra with published solution spectra measured between 3.5 and 5.5 eV.

Our gas-phase spectrum over the 3.5−10.7 eV range has many general similarities to the liquid-phase spectrum, but it shows more detailed structure and much better-resolved bands, where the liquid-phase bands are broad, as is the case for all bands above 4.2 eV. As expected, none of our assigned Rydberg band features are observed in the liquid-phase spectrum.

In the liquid phase the maximum absorption is at ∼6 eV with a cross section of ∼80 Mb, whereas we measure 193.6 Mb at our 6.218 eV maximum. This modification indicates a difference, between the liquid and gas phases, in the collective electron oscillations contributing to the absorption in this energy region marked by plasmon effects. The liquid-phase broad band between 6.9 and 8.8 eV corresponds to the more restricted background continuum between 7.5 and 8.6 eV in our gas-phase spectrum. However, the liquid-phase absorption cross-section maximum at 7.84 eV has a cross section of ∼60 Mb similar to that of our gas-phase maximum in this spectral region, $\sigma_{abs} = 62.15$ Mb. Furthermore, the absorption cross sections at 10.5 eV are similar in both liquid and gas, where $\sigma_{abs} \approx 70$ Mb.

IV. CONCLUSION

Quinoline absorption spectra were measured in the gas phase between 3.6 and 10.7 eV using the Aarhus synchrotron radiation facility photon source ASTRID2. A large number of sharp and broad spectral features was observed. These observations provide new information beyond those of previous studies that were mainly performed in solution and limited to an upper energy of ∼5.6 eV. TD-DFT calculations of quinoline of its ground state properties such as geometry, rotational constants, dipole moment, and vibrational frequencies agree well with experimental observations. The results of previous P−P−P quantum-mechanical computations of the valence-state energy levels and optical transition strengths, along with the results of our TD-DFT calculations of these quantities, were used to assign eight $\pi-\pi^*$ singlet $m^1A' \leftarrow 1^1A'$ valence electronic transitions of quinoline, along with their vibrational components. Only a small number of these electronic transitions were previously observed or assigned. The relative quality and trends of the P−P−P and DFT calculation results is discussed. Both are far from spectroscopic or even chemical accuracy but have proved useful in our assignments of the valence transitions. The $n-\pi^*$ transitions of these two compounds were too weak to be observed, as confirmed by our DFT calculations. It is suggested that some broad features, in particular, the intense broad band whose maximum is at 6.218 eV, may have plasmon-type collective π electron modes as important contributing components to their intensities.

Rydberg bands of quinoline were also observed for the first time and are analyzed into series converging to ground and to excited cation electronic states. Eight Rydberg series were assigned, two of which, R1 and R2 and their vibrational components, converge to the D_0 ion ground state. The extensive number of members of the R1 series enabled us to determine a value of 8.628 eV for the initial ionization energy of quinoline, a value more precise than previously published. The more limited third, fourth, and fifth Rydberg series, R3, R4, and R5, converge to the D_3 ion excited state at 10.623 eV, while the sixth, seventh, and eighth series, R6, R7, and R8, converge to the D_4 ion excited state at 11.355 eV.

A comparison of our gas-phase quinoline absorption spectrum with that measured for liquid quinoline in the 3.5−10.5 eV region[18] shows many general similarities in the valence-state region and the expected absence of Rydberg bands in the liquid phase.

Of the 137 measured features in our absorption spectrum 39 (28%) are not assigned. These nonassigned bands are mainly in the high-energy region. They are possibly higher-valence transitions or, more likely, Rydberg features to the numerous highly excited ion states, to and even beyond the D_4 level. We require more extended spectral measurements, up at least to 12 eV, to check these possibilities.

Finally we note that our spectral absorption data include absorption cross-section measurements in the VUV that can

provide useful new information for theoretical modeling of photochemical processes involving quinoline in planetary atmospheres and in the interstellar medium. Extensive spectroscopic searches for quinoline in the 75−158 GHz frequency range have been made toward the circumstellar envelopes of carbon-rich stars.[93] No positive results were obtained, but upper limits on the column densities were derived. The target stars were IRC + 10216, CRL 618, and CRL 2688. The latter two stars are protoplanetary nebulae in which molecules in the outflowing circumstellar envelope receive intense UV radiation from the star. In IRC + 10216, an AGB star, the inner dusty envelope is less subject to destructive UV irradiation, but molecules in the outward flow would enter regions of increasing UV flux and be subject to photodissociation.

To be more useful to astrophysical problems, our data need to be amplified by measurement of photoionization quantum yields of quinoline, going beyond rule-of-thumb estimations of energy-dependent ionization quantum yields.[94,95] This is of particular interest to assess the importance of photophysical and photochemical processes involving superexcited electronic states of the neutral molecule as a function of absorbed energy.[96] As an example, but using a rule-of-thumb method,[94] we estimate the quantum yield of ionization of quinoline to be $\gamma_i(13.6\ \text{eV}) = 0.54$ at the astrophysical HI region energy limit of 13.6 eV, so that ∼45% of the absorbed photon energy at 13.6 eV is retained for neutral molecule relaxation processes, including molecular dissociation. At an incident photon energy of 10.7 eV, the upper energy limit of our absorption spectral measurements, we estimate that ∼75% of the absorbed photon energy relaxes by nonionization processes.

AUTHOR INFORMATION

Corresponding Author

*Phone: 33-(0)145077561. E-mail: Sydney.Leach@obspm.fr.

ORCID

Sydney Leach: 0000-0002-2058-0247

Notes

The authors declare no competing financial interest.

ACKNOWLEDGMENTS

We thank N. Champion for technical assistance in the initial study of quinoline.

REFERENCES

(1) Landera, A.; Mebel, A. M. Mechanisms of Formation of Nitrogen-Containing Polycyclic Aromatic Compounds in Low-Temperature Environments of Planetary Atmospheres: A Theoretical Study. *Faraday Discuss.* **2010**, *147*, 479−494.

(2) Mattioda, A. L.; Hudgins, D. M.; Bauschlicher, C. W.; Rosi, M.; Allamandola, L. J. Infrared Spectroscopy of Matrix-Isolated Polycyclic Aromatic Compounds and Their Ions. 6. Polycyclic Aromatic Nitrogen Heterocycles. *J. Phys. Chem. A* **2003**, *107*, 1486−1498.

(3) Elsila, J. E.; Hammond, M. R.; Bernstein, M. P.; Sandford, S. A.; Zare, R. N. UV Photolysis of Quinoline in Interstellar Ice Analogs. *Meteorit. Planet. Sci.* **2006**, *41*, 785−796.

(4) Tielens, A. G. G. M. The Molecular Universe. *Rev. Mod. Phys.* **2013**, *85*, 1021−1081.

(5) Stoks, P. G.; Schwartz, A. W. Basic Nitrogen-Heterocyclic Compounds in the Murchison Meteorite. *Geochim. Cosmochim. Acta* **1982**, *46*, 309−315.

(6) Sephton, M. A. Organic Compounds in Carbonaceous Meteorites. *Nat. Prod. Rep.* **2002**, *19*, 292−311.

(7) Prajapati, S. M.; Patel, K. D.; Vekariya, R. H.; Panchal, S. N.; Patel, H. D. Recent Advances in the Synthesis of Quinolines: A Review. *RSC Adv.* **2014**, *4*, 24463−24476.

(8) Greenhill, J. V., Ed. *The Chemistry of Heterocyclic Compounds, Quinolines;* Wiley-Interscience, 1991; Vol. *32*.

(9) Marella, A.; Tanwar, O. P.; Saha, R.; Ali, M. R.; Srivastava, S.; Akhter, M.; Shaquiquzzaman, M.; Alam, M. M. Quinoline: A Versatile Heterocyclic. *Saudi Pharm. J.* **2013**, *21*, 1−12.

(10) Innes, K. K.; Ross, I. G.; Moomaw, W. R. Electronic States of Azabenzenes and Azanaphthalenes: A Revised and Extended Critical Review. *J. Mol. Spectrosc.* **1988**, *132*, 492−544.

(11) Ewing, G. W.; Steck, E. A. Absorption Spectra of Heterocyclic Compounds: Quinolinols and Isoquinolinols. *J. Am. Chem. Soc.* **1946**, *68*, 2181−2187.

(12) Purvis, J. The Absorption Spectra of Nicatine, Coniine and Quinoline as Vapours, Liquids and Solution. *J. Chem. Soc., Trans.* **1910**, *97*, 1035−1041.

(13) Amma, R. A.; Nair, K. P. R.; Singh, S. N. Infrared and Electronic Absorption Spectra of Quinoline. *Ind. J.Pure Appl.Chem.* **1969**, *7*, 567−569.

(14) Okajima, S.; Lim, E. C. Radiationless Transitions in Gaseous Nitrogen Heterocyclics: Energy Dependence of Internal Conversion in Quinoline and Isoquinoline. *J. Chem. Phys.* **1978**, *69*, 1929−1933.

(15) Hiraya, A.; Achiba, Y.; Kimura, K.; Lim, E. C. Identification of the Lowest Energy $n\pi^*$ States in Gas-Phase Polycyclic Monoazines: Quinoline and Isoquinoline. *J. Chem. Phys.* **1984**, *81*, 3345−3347.

(16) Favini, G.; Carrà, S.; Pierpaoli, V.; Polezzo, S.; Simonetta, M. Electronic Spectra of Mono-, Di- and Tri-Azines of the Naphthalene Series. *Nuovo Cimento* **1958**, *8*, 60−67.

(17) Müller, R.; Dörr, F. Absorptions- und Phosphoreszspektren der Mono- und der Diazanaphthaline (π-π-Phosphoreszenz nach n-π-Absorption bei den Diazanaphthalinen). *Zeitschr.f.Elektrochemie* **1959**, *63*, 1150−1156.

(18) MacRae, R. A.; Williams, M. W.; Arakawa, E. T. Optical Properties of Some Aromatic Liquids in the Vacuum Ultraviolet. *J. Chem. Phys.* **1974**, *61*, 861−865.

(19) Palmer, M. H.; Ridley, T.; Hoffmann, S. V.; Jones, N. C.; Coreno, M.; de Simone, M.; Grazioli, C.; Biczysko, M.; Baiardi, A.; Limão-Vieira, P. Interpretation of the Vacuum Ultraviolet Photoabsorption Spectrum of Iodobenzene by *ab initio* Computations. *J. Chem. Phys.* **2015**, *142*, 134302.

(20) Stratmann, R. E.; Scuseria, G. E.; Frisch, M. J. An Efficient Implementation of Time-Dependent Density-Functional Theory for the Calculation of Excitation Energies of Large Molecules. *J. Chem. Phys.* **1998**, *109*, 8218−8224.

(21) Cai, Z.-L.; Sendt, K.; Reimers, J. R. Failure of Density-Functional Theory and Time-Dependent Density-Functional Theory for Large Extended π Systems. *J. Chem. Phys.* **2002**, *117*, 5543−5549.

(22) Frisch, M. J.; Trucks, G. W.; Schlegel, H. B.; Scuseria, G. E.; Robb, M. A.; Cheeseman, J. R.; Scalmani, G.; Barone, V.; Mennucci, B.; Petersson, G. A.; et al. *Gaussian 09;* Gaussian, Inc.: Wallingford, CT, 2010.

(23) Yanai, T.; Tew, D. P.; Handy, N. C. A New Hybrid Exchange-Correlation Functional Using the Coulomb-Attenuating Method (CAM-B3LYP). *Chem. Phys. Lett.* **2004**, *393*, 51−57.

(24) Bandyopadhyay, I.; Manogaran, S. Force Field and Assignment of the Vibrational Spectra of Quinoline and Isoquinoline−An *ab initio* Study. *Indian J. Chem.* **2000**, *39A*, 189−195.

(25) Özel, A. E.; Büyükmurat, Y.; Akyüz, S. Infrared-Spectra and Normal-Coordinate Analysis of Quinoline and Quinoline Complexes. *J. Mol. Struct.* **2001**, *565*, 455−462.

(26) Kisiel, Z.; Desyatnyk, O.; Pszczółkowski, L.; Charnley, S. B.; Ehrenfreund, P. Rotational Spectra of Quinoline and Isoquinoline: Spectroscopic Constants and Electric Dipole Moments. *J. Mol. Spectrosc.* **2003**, *217*, 115−122.

(27) Moomaw, W. R.; Kleier, D. A.; Markgraf, J. H.; Thoman, J. W., Jr.; Ridyard, J. N. A. Strained Heterocyclic Systems.10. Photoelectron Spectra and Theoretical Studies of Bonding in Strained Quinolines. *J. Phys. Chem.* **1988**, *92*, 4892−4898.

(28) Pirali, O.; Kisiel, Z.; Goubet, M.; Gruet, S.; Martin-Drumel, M. A.; Cuisset, A.; Hindle, F.; Mouret, G. Rotation-Vibration Interactions in the Spectra of Polycyclic Aromatic Hydrocarbons: Quinoline as a Test-Case Species. *J. Chem. Phys.* **2015**, *142*, 104310.
(29) Martin-Drumel, M. A.; Pirali, O.; Loquais, Y.; Falvo, C.; Bréchignac, P. Lowest Energy Vibrational Modes of Some Natphthalene Derivatives: Azulene, Quinoline, Isoquinoline−Experiment and Theory. *Chem. Phys. Lett.* **2013**, *557*, 53−58.
(30) Buckingham, A. D.; Chau, J. Y. H.; Freeman, H. C.; Le Fèvre, R. J. W.; Narayana Rao, D. A. A. S.; Tardif, J. The Dipole Moments of Pyridine, Quinoline, and Isoquinoline as Vapours and as Solutes. *J. Chem. Soc.* **1956**, *0*, 1405−1411.
(31) Ebenso, E. E.; Kabanda, M. M.; Arslan, T.; Aracoglu, M. S.; Kandemirli, F.; Murulana, L. C.; Singh, A. K.; Shukla, S. K.; Hammouti, B.; Khaled, K. F.; et al. Quantum Chemical Investigations on Quinoline Derivatives as Effective Inhibitors for Mild Steel in Acid Medium. *Int.J.Electrochem.Sci.* **2012**, *7*, 5643−5676.
(32) Wait, S. C., Jr.; McNerney, J. C. Vibrational Spectra and Assignments for Quinoline and Isoquinoline. *J. Mol. Spectrosc.* **1970**, *34*, 56−77.
(33) Hamprecht, F. A.; Cohen, A. J.; Tozer, D. J.; Handy, N. C. Development and Assessment of New Exchange-Correlation Functionals. *J. Chem. Phys.* **1998**, *109*, 6264−6271.
(34) Scott, A. P.; Radom, L. Harmonic Vibrational Frequencies: An Evaluation of Hartree-Fock, Møller-Plesset, Quadratic Configuration Interaction, Density Functional Theory, and Semiempirical Scale Factors. *J. Phys. Chem.* **1996**, *100*, 16502−16513.
(35) Barone, V. Anharmonic Vibrational Properties by a Fully Automated Second-Order Perturbative Approach. *J. Chem. Phys.* **2005**, *122*, 014108.
(36) Wasserman, A.; Maitra, N. T.; Burke, K. Accurate Rydberg Excitations from the Local Density Approximation. *Phys. Rev. Lett.* **2003**, *91*, 263001.
(37) Burke, K.; Werschnik, J.; Gross, E. K. U. Time-Dependent Density Functional Theory: Past, Present, and Future. *J. Chem. Phys.* **2005**, *123*, 062206.
(38) Baba, H.; Yamazaki, I. Interpretation of Electronic Spectra by Configuration Analysis. Absorption Spectra of Azanaphthalenes. *J. Mol. Spectrosc.* **1972**, *44*, 118−130.
(39) Nishimoto, K. The Variable Core Approach in the SCF MO Calculation of Heteroatomic Systems. *Theoret.chim.Acta (Berl.)* **1968**, *10*, 65−72.
(40) Tinland, B. SCF MO Calculations of Ultraviolet Electronic Spectra of Azanaphthalenes with the Variable Beta Approximation. *Theoret.chim.Acta (Berl.)* **1967**, *8*, 361−366.
(41) Ridley, J. E.; Zerner, M. C. The Calculated Spectra of the Azanaphthalenes. *J. Mol. Spectrosc.* **1974**, *50*, 457−473.
(42) Wagner, R. W.; Hochmann, P.; El-Bayoumi, M. A. LCI Pariser-Parr-Pople Calculations of π-Electron Systems in Nitrogen-Heterocyclic Molecules. Correlation with Spectral Data. *J. Mol. Spectrosc.* **1975**, *54*, 167−181.
(43) Mataga, N. A Theory of the Electronic Spectra of Nitrogen Heterocycles: Azanaphthalenes and Azaanthracenes. *Z. Phys. Chem.* **1958**, *18*, 285−302.
(44) Goodman, L.; Harrell, R. W. Calculation of $n-\pi^*$ Transition Energies in N-Heterocyclic Molecules by a One-Electron Approximation. *J. Chem. Phys.* **1959**, *30*, 1131−1138.
(45) Reichardt, C. *Solvents and Solvent Effects in Organic Chemistry*, 2nd ed.; VCH: Weinheim, Germany, 1988.
(46) Bensasson, R. V.; Bienvenue, E.; Dellinger, M.; Leach, S.; Seta, P. C_{60} in Model Biological Systems. A Visible-UV Absorption Study of Solvent-Dependent Parameters and Solute Aggregation. *J. Phys. Chem.* **1994**, *98*, 3492−3500.
(47) Sassara, A.; Zerza, G.; Chergui, M.; Leach, S. Absorption Wavelengths and Bandwidths for Interstellar Searches of C_{60} in the 2400−4100 Å Region. *Astrophys. J., Suppl. Ser.* **2001**, *135*, 263−273.
(48) Crépin, C.; Dubois, V.; Goldfarb, F.; Chaput, F.; Boilot, J. P. A Site-Selective Spectroscopy of Naphthalene and Quinoline in TEOS/MTEOS Xerogels. *Phys. Chem. Chem. Phys.* **2005**, *7*, 1933−1938.
(49) Zimmerman, H.; Joop, N. Polarisation der Elektronenbanden von Aromaten. 3. Mitteillung: Chinolin, Isochinolin, Indol. *Zeitschr.f.Elektrochem.* **1961**, *65*, 61−65.
(50) Anton, M. F.; Moomaw, W. R. Luminescence and Hydrogen Bonding in Quinoline and Isoquinoline. *J. Chem. Phys.* **1977**, *66*, 1808−1818.
(51) Coppens, G.; Nasielski, J. Propriétés Physico-chimiques de Composés à Caractère Aromatique. *Bull. Soc. Chim. Belg.* **1961**, *70*, 136−144.
(52) Bellamy, L. J. *The Infrared Spectra of Complex Molecules;* Methuen: London, England, 1954.
(53) Platt, J. R. Classification of Spectra of Cata-Condensed Hydrocarbons. *J. Chem. Phys.* **1949**, *17*, 484−495.
(54) Kaito, A.; Hatano, M. Experimental and Theoretical Studies on the Magnetic Circular Dichroism of Azanaphthalenes. Use of the CNDO/S-CI Approximation. *J. Am. Chem. Soc.* **1978**, *100*, 4037−4044.
(55) Vašák, M.; Whipple, M. R.; Michl, J. Magnetic Circular Dichroism of Cyclic π-Electron Systems.7. Aza Analogues of Naphthalene. *J. Am. Chem. Soc.* **1978**, *100*, 6838−6843.
(56) Vaida, V.; Robin, M. B.; Kuebler, N. A. A Note on the Elusive $^1E_{2g}$ State in the Two-Photon Spectrum of Benzene. *Chem. Phys. Lett.* **1978**, *58*, 557−560.
(57) Koch, E. E.; Otto, A. Vacuum Ultraviolet and Electron Energy Loss Spectroscopy of Gaseous and Solid Organic Compounds. *Int. J. Radiat. Phys. Chem.* **1976**, *8*, 113−150.
(58) Bernadotte, S.; Evers, F.; Jacob, C. R. Plasmons in Molecules. J. *J. Phys. Chem. C* **2013**, *117*, 1863−1878.
(59) Krauter, C. M.; Schirmer, J.; Jacob, C. R.; Pernpointner, M.; Dreuw, A. Plasmons in Molecules: Microscopic Characterization Baszd on Orbital Transitions and Moment Conservation. *J. Chem. Phys.* **2014**, *141*, 104101.
(60) Krauter, C. M.; Bernadotte, S.; Jacob, C. R.; Pernpointner, M.; Dreuw, A. Identification of Plasmons in Molecules with Scaled Ab Initio Approaches. *J. Phys. Chem. C* **2015**, *119*, 24564−24573.
(61) Koch, E. E.; Otto, A.; Radler, K. The Vacuum Ultraviolet Spectrum of Naphthalene Vapour for Photon Energies from 5 to 30 eV. *Chem. Phys. Lett.* **1972**, *16*, 131−135.
(62) Guidez, E. B.; Aikens, C. M. Origin and TDDFT Benchmarking of the Plasmon Resonance in Acenes. *J. Phys. Chem. C* **2013**, *117*, 21466−21475.
(63) Casida, M. E.; Jamorski, C.; Casida, K. C.; Salahub, D. Molecular Excitation Energies to High-Lying Bound States from Time-Dependent Density-Functional Response Theory: Characterization and Correction of the Time-Dependent Local Density Approximation. *J. Chem. Phys.* **1998**, *108*, 4439−4449.
(64) Furche, F.; Ahlrichs, R. Adiabatic Time-Devpendent Density Functional Methods for Excited State Properties. *J. Chem. Phys.* **2002**, *117*, 7433−7447.
(65) Silva-Junior, M. R.; Schreiber, M.; Sauer, S. P. A.; Thiel, W. J. Benchmarks for Electronically Excited States: Time-Dependent Density Functional Theory and Density Functional Theory Based Multireference Configuration Interaction. *J. Chem. Phys.* **2008**, *129*, 104103.
(66) Goerigk, L.; Moellmann, J.; Grimme, S. Computation of Accurate Excitation Energies for Large Organic Molecules with Double-Hybrid Density Functionals. *Phys. Chem. Chem. Phys.* **2009**, *11*, 4611−4620.
(67) Jacquemin, D.; Wathelet, V.; Perpète, E. A.; Adamo, C. Extensive TD-DFT Benchmark: Singlet-Excited States of Organic Molecules. *J. Chem. Theory Comput.* **2009**, *5*, 2420−2435.
(68) Jacquemin, D.; Perpète, E. A.; Ciofini, B.; Adamo, C.; Valero, R.; Zhao, Y.; Truhlar, D. G. On the Performances of the M06 Family of Density Functionals for Electronic Excitation Energies. *J. Chem. Theory Comput.* **2010**, *6*, 2071−2085.
(69) Caricato, M.; Trucks, G. W.; Frisch, M. J.; Wiberg, K. B. Electronic Transition Energies: Study of the Performance of a Large Range of Single Reference Density Functional and Wave Function

Methods on Valence and Rydberg States Compared to Experiment. *J. Chem. Theory Comput.* **2010**, *6*, 370−383.
(70) Silva-Junior, M. R.; Schreiber, M.; Sauer, S. P. A.; Thiel, W. Benchmarks of Electronically Excited States: Basis Set Effects on CAPSPT2 Results. *J. Chem. Phys.* **2010**, *133*, 174318.
(71) Isegawa, M.; Peverati, R.; Truhlar, D. G. Performance of Recent and High-Performance Approximate Density Functionals for Time-Dependent Functional Theory Calculations of Valence and Rydberg Electronic Transition Energies. *J. Chem. Phys.* **2012**, *137*, 244104.
(72) Leang, S. S.; Zahariev, F.; Gordon, M. S. Benchmarking the Performance of Time-Dependent Density Functional Methods. *J. Chem. Phys.* **2012**, *136*, 104101.
(73) Isegawa, M.; Truhlar, D. G. Valence Excitation Energies of Alkenes, Carbonyl Compounds, and Azabenzenes by Time-Dependent Density Functional Theory: Linear Response of the Ground State Compared to Collinear and Noncollinear Spin-Flip TDDFT with the Tamm-Dancoff Approximation. *J. Chem. Phys.* **2013**, *138*, 134111.
(74) Grimme, S.; Parac, M. Substantial Errors from TDDFT for the Calculation of Excited States of Large Systems. *ChemPhysChem* **2003**, *4*, 292−295.
(75) Prlj, A.; Sandoval-Salinas, M. E.; Casanova, D.; Jacquemin, D.; Corminboeuf, C. Low-Lying $\pi\pi^*$ States of Heteroatomic Molecules: A Challenge for Excited State Methods. *J. Chem. Theory Comput.* **2016**, *12*, 2652−2660.
(76) Eland, J. H. D.; Danby, C. J. Inner Ionization Potentials of Aromatic Compounds. *Z. Naturforsch., A: Phys. Sci.* **1968**, *23a*, 355−357.
(77) Ahmed, A. A.; Julliard, M.; Chanon, F.; Chanon, M.; Gracian, F.; Pfister-Guillouzo, G. Photoelectron Spectroscopy of Quinoline Derivatives. Correlation of Experimental Ionization Potentials with Calculated Molecular Energies. *Spectrochim. Acta, Part A* **1997**, *53*, 335−343.
(78) Brogli, F.; Heilbronner, E.; Kobayashi, T. Photoelectron Spektra of Azabenzenes and Azanaphthalenes: A Reinvestigation of Azanaphthalenes by High-Resolution Photoelectron Spectroscopy. *Helv. Chim. Acta* **1972**, *55*, 274−288.
(79) Dewar, M. J. S.; Worley, S. D. Photoelectron Spectra of Molecules.II. The Ionization Potentials of Azabenzenes and Azanaphthalenes. *J. Chem. Phys.* **1969**, *51*, 263−267.
(80) Bouwman, J.; Sztáray, B.; Oomens, J.; Hemberger, P.; Bodi, A. Dissociative Photoionization of Quinoline and Isoquinoline. *J. Phys. Chem. A* **2015**, *119*, 1127−1136.
(81) Yencha, A. J.; El-Sayed, M. A. Lowest Ionization Potentials of Some Nitrogen Heterocyclics. *J. Chem. Phys.* **1968**, *48*, 3469−3475.
(82) Leach, S.; Jochims, H.-W.; Baumgärtel, H.; Champion, N. VUV Dissociative Photoionization of Quinoline in the 7−26 eV Photon Energy Range. *Z. Phys. Chem.* **2018**, *232*, 845−881.
(83) Dryza, V.; Sanelli, J. A.; Robertson, E. G.; Bieske, E. J. Electronic Spectra of Gas-Phase Polycyclic Aromatic Nitrogen Heterocycle Cations: Isoquinoline and Quinoline. *J. Phys. Chem. A* **2012**, *116*, 4323−4329.
(84) Hochmann, P.; Wang, H. T.; Felps, W. S.; Foster, S.; McGlynn, S. P. In *Chemical Spectroscopy and Photochemistry in the Vacuum-Ultraviolet;* Sandorfy, C., Ausloos, P. J., Robin, M. D., Eds.; D.Reidel: Dordrecht, Netherlands, 1974; pp 385−393.
(85) Angus, J. G.; Morris, G. C. The Lowest Free Molecule Rydberg Transition of Naphthalene. *Aust. J. Chem.* **1971**, *24*, 173−177.
(86) Alvaro Galué, H.; Pirali, O.; Oomens, J. Gas-Phase Infrared Spectra of Cationized Nitrogen-Substituted Polycyclic Aromatic Hydrocarbons. *Astron. Astrophys.* **2010**, *517*, A15.
(87) Mayer, P. M.; Blanchet, V.; Joblin, C. J. Threshold Photoelectron Study of Naphthalene, Anthracene, Pyrene, 1,2-Dihydronaphthalene, and 9,10-Dihydroanthracene. *J. Chem. Phys.* **2011**, *134*, 244312.
(88) Bell, S. The spectra of H_2O and D_2O in the vacuum ultraviolet. *J. Mol. Spectrosc.* **1965**, *16*, 205−213.
(89) Yoshino, K.; Esmond, J. R.; Parkinson, W. H.; Ito, K.; Matsui, T. Absorption Cross Section Measurements of Water Vapor in the Wavelength Region 120 to 188 nm. *Chem. Phys.* **1996**, *211*, 387−391.
(90) Watanabe, K.; Zelikoff, M. Absorption Coefficients of Water Vapor in the Vacuum Ultraviolet. *J. Opt. Soc. Am.* **1953**, *43*, 753−755.
(91) Gürtler, P.; Saile, V.; Koch, E. E. Rydberg Series in the Absorption Spectra of H_2O and D_2O in the Vacuum Ultraviolet. *Chem. Phys. Lett.* **1977**, *51*, 386−391.
(92) Chan, W. F.; Cooper, G.; Brion, C. E. The electronic spectrum of water in the discrete and continuum regions. Absolute optical oscillator strengths for photoabsorption (6−200 eV). *Chem. Phys.* **1993**, *178*, 387−400.
(93) Charnley, S. B.; Kuan, Y.-J; Huang, H.-C.; Botta, O.; Butner, H. M.; Cox, N.; Despois, D.; Ehrenfreund; Kisiel, Z.; Lee, Y.-Y.; et al. Astronomical Searches for Nitrogen Heterocycles. *Adv. Space Res.* **2005**, *36*, 137−135.
(94) Jochims, H. W.; Baumgärtel, H.; Leach, S. Photoionization Quantum Yields of Polycyclic Hydrocarbons. *Astron. Astrophys.* **1996**, *314*, 1003−1009.
(95) Le Page, V.; Snow, T. P.; Bierbaum, V. M. Hydrogenation and Charge States of PAHS in [Diffuse Clouds. I. Development of a Model. *Astrophys. J., Suppl. Ser.* **2001**, *132*, 233−251.
(96) Hatano, Y. Interaction of VUV Photons with Molecules. Spectroscopy and Dynamics of Molecular Superexcited States. *J. Electron Spectrosc. Relat. Phenom.* **2001**, *119*, 107−125.